

Rethinking Meta-Learning from a Learning Lens

Jingyao Wang^{1,2} Wenwen Qiang^{1,2} Chuxiong Sun^{1,2} Changwen Zheng^{1,2} Jiangmeng Li^{1,2}

Abstract

Meta-learning seeks to learn a well-generalized model initialization from training tasks to solve unseen tasks. From the “learning to learn” perspective, the quality of the initialization is modeled with one-step gradient decent in the inner loop. However, contrary to theoretical expectations, our empirical analysis reveals that this may expose meta-learning to underfitting. To bridge the gap between theoretical understanding and practical implementation, we reconsider meta-learning from the “Learning” lens. We propose that the meta-learning model comprises two interrelated components: parameters for model initialization and a meta-layer for task-specific fine-tuning. These components will lead to the risks of overfitting and underfitting depending on tasks, and their solutions—fewer parameters vs. more meta-layer—are often in conflict. To address this, we aim to regulate the task information the model receives without modifying the data or model structure. Our theoretical analysis indicates that models adapted to different tasks can mutually reinforce each other, highlighting the effective information. Based on this insight, we propose TRLearner, a plug-and-play method that leverages task relation to calibrate meta-learning. It first extracts task relation matrices and then applies relation-aware consistency regularization to guide optimization. Extensive theoretical and empirical evaluations demonstrate its effectiveness.

1. Introduction

Meta-learning, also known as “learning to learn”, acquires knowledge from multiple tasks and then adapts to unseen tasks. Recently, meta-learning has demonstrated tremendous success in various applications, such as affective com-

¹Institute of Software Chinese Academy of Sciences, Beijing, China ²University of the Chinese Academy of Sciences, Beijing, China. Correspondence to: Wenwen Qiang <qiangwenwen@iscas.ac.cn>.

puting (Li et al., 2023), image classification (Chen et al., 2021), and robotics (Schrum et al., 2022).

This work focuses on meta-learning methods based on bi-level optimization (Verma et al., 2020; Hospedales et al., 2021). The main approaches include optimization-based (Finn et al., 2017; Nichol & Schulman, 2018; Raghu et al., 2019a;b) and metric-based methods (Snell et al., 2017; Sung et al., 2018). These methods typically aim to learn an effective model initialization, which is subsequently fine-tuned for downstream tasks to produce task-specific models. Let the initialized model be \mathcal{F}_θ , and the task-specific model for the i -th task be f_θ^i . The training data for each task is divided into a support set and a query set (analogous to the training and testing sets in traditional machine learning). Then, the meta-learning process includes two steps: (i) The inner loop, referred to as “to learn”, aims to derive f_θ^i through a single gradient descent step based on \mathcal{F}_θ and the support set; (ii) The outer loop, referred to as “learning”, updates \mathcal{F}_θ based on the performance of f_θ^i on the query set, again using gradient descent. Notably, the “one gradient descent step” reflects the proximity of \mathcal{F}_θ and f_θ^i . The bi-level learning process enforces a constraint that the model obtained after one-step gradient descent should perform well on the given task. That is, based on \mathcal{F}_θ , a single gradient descent step should produce the optimal f_θ^i . Thus, the “quality” of the initialized model is primarily modeled as “one-step gradient descent”, as the “best” \mathcal{F}_θ is the one closest to optimal f_θ^i .

Both theoretically and methodologically, meta-learning based on bi-level optimization has made significant progress (Chen et al., 2019; Finn et al., 2017; Raghu et al., 2019a). However, understanding meta-learning from “learning a good initialization model” has a gap with practical implementation. First, there is a logical paradox between the objective of meta-learning and its actual implementation during the training phase. According to Eq.1, the constraints aim to obtain the optimal task-specific model. Clearly, achieving this goal with only a single gradient descent step is difficult. From the “good initialization model” perspective, however, “one gradient descent step” is indeed a crucial component. Second, as shown in (Flennerhag et al., 2021), distilling the information contained in the parameters of task-specific models obtained after “multiple gradient descent steps” into those obtained after “one gradient descent step” can significantly enhance meta-learning perfor-

mance on downstream tasks. Our experiments in **Figure 2** also demonstrate that meta-learning optimization relying on single-step gradient descent is insufficient. These pieces of evidence show that understanding meta-learning from learning a “good initialization model” is inadequate.

To bridge the above gap, we rethink meta-learning from the “Learning” lens to unify the theoretical understanding with practical implementation (**Subsection 3.1**). Different from the previous understanding of “learning a good initialization”, we focus on the viewpoint that meta-learning can be explained as learning a model \mathcal{F}_θ that given any task τ_i , outputs a task-specific model f_θ^i that performs well, i.e., $\mathcal{F}_\theta(\tau_i) = f_\theta^i$. **The central challenge lies in modeling \mathcal{F}_θ , however, existing work does not discuss this, and this paper focuses on this.** A natural idea is to employ a large MLP to construct \mathcal{F}_θ , but the required parameters could be prohibitively large. Drawing inspiration from the enhanced representational power of nonlinear functions (Haarhoff & Buys, 1970; Schwartz, 1969), this issue can be solved by incorporating a nonlinear layer. We use gradient optimization to model this nonlinear layer, called “meta-layer”. Then, we get $\mathcal{F}_\theta - \frac{\partial \mathcal{L}}{\partial \theta} = f_\theta^i$. Compared with MLP-based modeling, the meta-layer reduces the parameters of \mathcal{F}_θ while improving representational capacity. \mathcal{F}_θ can be regarded as consisting of the model initialization layers and the meta-layer (**Figure 1**). This modeling has two advantages. First, it aligns with the bi-level optimization: (i) Inner-loop: output f_θ^i via $\mathcal{F}_\theta - \frac{\partial \mathcal{L}}{\partial \theta} = f_\theta^i$, (ii) Outer-loop: update \mathcal{F}_θ by evaluating the performance of multiple outputs f_θ^i . Second, it is more flexible which bridges the gap between theory and implementation. Specifically, for few-shot tasks, a single meta-layer is used to avoid over-fitting; for complex tasks, more meta-layers can be used to avoid overfitting.

Under our understanding, the key issue is determining how many meta-layers to use for \mathcal{F}_θ . Due to task diversity, it is difficult to find a fixed number of meta-layers to suit all tasks. This results in meta-learning models facing modeling errors, i.e., errors caused by model selection (Mohri, 2018) that are difficult to eliminate. To address this, we propose a proxy to balance the modeling errors. According to (LeCun et al., 2015), the key to the accurate prediction of models is to fully learn important features of each task. Following (Pearl, 2009), important features refer to those directly related to labels and shared by samples within the same class. Without considering other errors such as data sampling, the presence of modeling errors may directly affect the ability of the model to extract important features, e.g., underfitting or overfitting of the model can lead to biased learning of important features. Thus, the proxy aims to constrain the model to capture important features of different tasks without changing the model structure. Through theoretical analysis (**Theorem 3.1**), we prove that the classifier for a specific task in meta-learning can leverage features

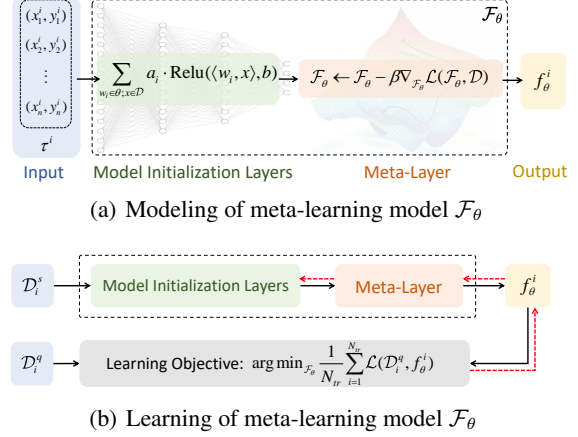


Figure 1. Reformulation of meta-learning model \mathcal{F}_θ .

from similar tasks to promote classification. Thus, a good meta-learning model \mathcal{F}_θ should produce similar outputs for task-specific models on similar tasks. **This inspires us to develop a method for extracting task relations and integrating them into meta-learning to make the model focus on important task features, achieving the proxy.**

Motivated by the above insight, we finally propose Task Relation Learner (TRLearner), a plug-and-play method that leverages task relations to calibrate meta-learning. It first computes a task relation matrix based on task-specific meta-data. These meta-data are extracted via an adaptive sampler to make it contain discriminative information. Then, it uses a relation-aware consistency regularization to calibrate meta-learning. The regularization term constrains the meta-learning model to produce similar performance after fine-tuning on similar tasks with the obtained matrix, thereby enhancing the model’s focus on important features. Theoretical analyses demonstrate that after the introduction of TRLearner, the meta-learning model achieves smaller excess risk and better generalization performance.

The main contributions are: **(i)** We rethink meta-learning from the “learning” lens to bridge the gap between theoretical understanding and practical implementation (**Section 3**). **(ii)** We propose TRLearner, a plug-and-play method that leverages task relations to calibrate meta-learning (**Section 4**). **(iii)** Theoretical and empirical evaluations demonstrate the effectiveness of TRLearner (**Sections 5 and 6**).

2. Problem Formulation and Challenge

Meta-learning aims to learn an effective $\mathcal{F}_\theta = h \circ g$ that can adapt to unseen tasks. Here, g is the feature extractor and h is the classifier. A meta-learning dataset is divided into two parts, e.g., meta-training task dataset \mathcal{D}_{tr} and meta-test task dataset \mathcal{D}_{te} , these two are all assumed to be sampled from an identical task distribution $p(\mathcal{T})$. Moreover, \mathcal{D}_{tr} and \mathcal{D}_{te} have no class overlap. During training, each batch

includes N_{tr} tasks, denoted as $\{\tau_i\}_{i=1}^{N_{tr}} \in \mathcal{D}_{tr}$. Each task τ_i comprises a support set $\mathcal{D}_i^s = \{(x_{i,j}^s, y_{i,j}^s)\}_{j=1}^{N_i^s}$ and a query set $\mathcal{D}_i^q = \{(x_{i,j}^q, y_{i,j}^q)\}_{j=1}^{N_i^q}$. Here, $(x_{i,j}, y_{i,j})$ is the sample and corresponding label, N_i is the number of samples.

The learning mechanism of meta-learning can be regarded as a bi-level optimization process. In the first level, it fine-tunes \mathcal{F}_θ on task τ_i with the support set \mathcal{D}_i^s , obtaining the task-specific model f_θ^i through one-step gradient descent:

$$f_\theta^i \leftarrow \mathcal{F}_\theta - \alpha \nabla_{\mathcal{F}_\theta} \mathcal{L}(\mathcal{D}_i^s, \mathcal{F}_\theta), \quad (1)$$

where $\mathcal{L}(\mathcal{D}_i^s, \mathcal{F}_\theta) = \frac{1}{N_i^s} \sum_{j=1}^{N_i^s} y_{i,j}^s \log \mathcal{F}_\theta(x_{i,j}^s)$,

where α denotes the learning rate. In the second level, meta-learning updates the model \mathcal{F}_θ using the obtained task-specific models f_θ^i and the query sets \mathcal{D}_i^q of multiple tasks:

$$\mathcal{F}_\theta \leftarrow \mathcal{F}_\theta - \beta \nabla_{\mathcal{F}_\theta} \frac{1}{N_{tr}} \sum_{i=1}^{N_{tr}} \mathcal{L}(\mathcal{D}_i^q, f_\theta^i), \quad (2)$$

where $\mathcal{L}(\mathcal{D}_i^q, f_\theta^i) = \frac{1}{N_i^q} \sum_{j=1}^{N_i^q} y_{i,j}^q \log f_\theta^i(x_{i,j}^q)$,

where β is the learning rate. Note that f_θ^i is derived by taking the derivative of \mathcal{F}_θ , making f_θ^i a function of \mathcal{F}_θ . Consequently, updating \mathcal{F}_θ as described in Eq.2 can be interpreted as computing the second derivative of \mathcal{F}_θ .

Generally, existing methods (Finn et al., 2017; Verma et al., 2020) understand the aforementioned bi-level optimization process in meta-learning from the perspective of “learning a good initialization”. Specifically, “Learning a good initialization” requires the meta-learning model to adapt quickly to tasks. Achieving this hinges on the effective realization of “adapt quickly” which can be modeled as the “one gradient descent” in the first level. Therefore, through this understanding, we can obtain the “one gradient descent” is the key to the implementation of a “good model initialization”.

Existing Challenge. However, there exists a gap between the above understanding and practical implementation. Specifically, empirical evidence suggests that existing methods are prone to underfitting (Wang et al., 2024a), which occurs when first-level updates are inadequate, e.g., one-step gradient descent. However, the above formulation views the “one gradient descent” as essential for achieving a good initialization, rather than a potential cause of underfitting. Second, according to (Flennerhag et al., 2021), in scenarios like reinforcement learning, transferring the information from task-specific models learned through future steps, i.e., “multiple gradient descent steps”, into those obtained from “a single gradient descent step” enhances meta-learning performance on downstream tasks. Thus, the current understanding of meta-learning remains limited.

Empirical Evidence. To verify the limitations of existing methods that understand meta-learning from learning a “good initialization model”, we conduct a toy experiment. It

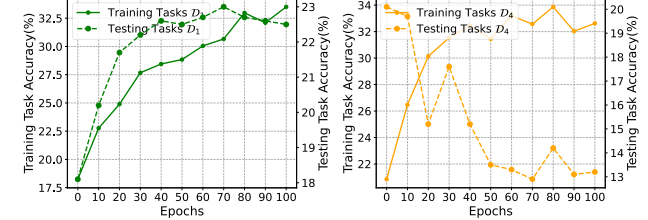


Figure 2. Motivating evidence. **Left:** results of models trained on \mathcal{D}_1 (0.74), and **Right:** results of models trained on \mathcal{D}_4 (0.29).

evaluates the performance of meta-learning models relying on a single “meta-layer” across different tasks, i.e., whether face overfitting and underfitting according to tasks. Specifically, we first sample 20 sets of tasks from miniImagenet (Vinyals et al., 2016) based on (Wang et al., 2024a). We select the top two tasks with the highest scores as $\mathcal{D}_1 - \mathcal{D}_2$, and the bottom two as $\mathcal{D}_3 - \mathcal{D}_4$. The higher the sampling scores, the more complex the task. Then, we perform four rounds of data augmentation on $\mathcal{D}_1 - \mathcal{D}_2$. Next, we train MAML (Finn et al., 2017) on these sets of tasks, i.e., fine-tuning the model with one gradient descent step in the inner loop. We record the training loss and the accuracy on previously unseen test tasks. From Figure 2, we observe that: (i) models trained on \mathcal{D}_4 exhibit an inflection point in training loss but perform worse on the test set, indicating overfitting; (ii) models on \mathcal{D}_1 show lower performance after convergence and the test performance gradually improves, indicating underfitting. These results demonstrate that existing methods do face the limitations of overfitting and underfitting depending on tasks. See Appendix H for more details.

3. Problem Analysis and Motivation

To unify theoretical understanding with practical implementation, we revisit meta-learning from the “learning” lens (**Subsection 3.1**). Based on the analyses, we then conduct theoretical analyses (**Subsection 3.2**) to explore how to eliminate the limitations of existing meta-learning methods.

3.1. Rethink Meta-Learning from “Learning” Lens

We focus on the view that meta-learning is to learn a model \mathcal{F}_θ : given any task τ_i , it can output a task-specific model f_θ^i that performs well, i.e., $\mathcal{F}_\theta(\tau_i) = f_\theta^i$. The dataset for task τ_i is \mathcal{D}_i , then the desired f_θ^i is to achieve $\min \mathbb{E}_{(x,y) \in \mathcal{D}_i} [\ell(f_\theta^i(x), y)]$. Having the forms of τ_i and f_θ^i , the central challenge lies in modeling \mathcal{F}_θ , a topic not addressed in existing literature, which this paper focuses on.

A natural idea is to employ an MLP to construct \mathcal{F}_θ since MLP is capable of approximating any continuous function using a series of linear layers (Pinkus, 1999; Taud & Mas, 2018). However, the required MLP would be extraordinarily large, affecting applicability. First, the parameter count is substantial: for complex tasks, the larger parameter count

of f_θ^i results in an increase in the parameters of \mathcal{F}_θ . Second, the capacity of the MLP is also considerable: MLPs rely on linear layers to fulfill the need for meta-learning that handles various tasks demands a high representational capability.

To address the above limitations, we aim to reduce the network parameters without compromising its representational ability, thus better modeling \mathcal{F}_θ . According to (Haarhoff & Buys, 1970; Schwartz, 1969), to improve the representational capability of the network, one approach is to use multiple linear layers, while another is to introduce fewer nonlinear layers. For instance, to represent the unit circle, we can use either an infinite series of linear equations $y = wx + b$ or one nonlinear equation $x^2 + y^2 = 1$. Based on this, we propose introducing nonlinear layers to replace the original linear layers, reducing the parameter count of the network while preserving its representational capability.

Specifically, we propose using the gradient optimization function to implement the nonlinear layer, called the “meta-layer”. Compared to the Relu-based function (Daubechies et al., 2022), the computational complexity of the nonlinear gradient optimization function is higher (Watrous, 1988). Then, the meta-learning model \mathcal{F}_θ can be modeled as consisting of the model initialization layers and a meta-layer (**Figure 1(a)**). The model initialization layers can be seen as composed of multiple interconnected neurons, e.g., ResNet50. These neurons work together through weighted inputs $\langle \omega_i, x \rangle$, bias term b , the activation function ReLU, and scaling factor a_i , as: $\mathcal{F}_\theta : \sum_{\omega_i \in \theta, x \in \mathcal{D}} a_i \cdot \text{ReLU}(\langle \omega_i, x_i \rangle, b)$. The construction of the meta-layer is motivated by the first-level optimization within meta-learning. It is defined by the loss function $\mathcal{L}(\cdot)$, gradient computation $\nabla_{\mathcal{F}_\theta}$, and learning rate β , as: $\mathcal{F}_\theta \leftarrow \mathcal{F}_\theta - \beta \nabla_{\mathcal{F}_\theta} \mathcal{L}(\mathcal{F}_\theta, \mathcal{D})$. From this implementation, the learnable parameters in the meta-layer are the same as in model initialization layers. Therefore, the learnable parameters of \mathcal{F}_θ are those in model initialization layers. For the learning process (**Figure 1(b)**), the dataset contains one meta-training task dataset and one meta-test task dataset. Each task τ_i consists of a support set \mathcal{D}_i^s and a query set \mathcal{D}_i^q . First, the model \mathcal{F}_θ takes \mathcal{D}_i^s as input and outputs task-specific model f_θ^i , i.e., $\mathcal{F}_\theta(\tau_i) = f_\theta^i$. Then, we evaluate the performance of multiple outputs, i.e., the loss $\mathcal{L}(\mathcal{D}_i^q, f_\theta^i)$ on each query set \mathcal{D}_i^q , and update \mathcal{F}_θ . The objective is:

$$\arg \min_{\mathcal{F}_\theta} \frac{1}{N_{tr}} \sum_{i=1}^{N_{tr}} \mathcal{L}(\mathcal{D}_i^q, f_\theta^i). \quad (3)$$

This modeling achieves two advantages. First, it aligns with the bi-level optimization of meta-learning: (i) The forward computation process (black line in **Figure 1(b)**) is to obtain the task-specific model, i.e., $F_\theta - \frac{\partial \mathcal{L}}{\partial \theta} = f_\theta^i$ (inner-loop). (ii) The back-propagation process (red line in **Figure 1(b)**) updates θ using multiple f_θ^i (outer-loop). Second, it unifies

the theoretical understanding with practical implementation, which is more flexible. Specifically, we can flexibly adjust the number of meta-layers to improve model performance: (i) In few-shot tasks, \mathcal{F}_θ uses only one meta-layer to balance the parameters and the data volume, avoiding overfitting. (ii) In complex tasks, \mathcal{F}_θ uses more meta-layers to support more sufficient learning, avoiding underfitting.

3.2. Theoretical Insights: Method Motivation

Based on the above analyses, the key to improving meta-learning is determining the appropriate number of meta-layers. The optimal number of meta-layers varies across tasks, making it difficult to define a fixed number suitable for all meta-learning tasks. Consequently, the persistent modeling errors (Mohri, 2018) from meta-layer depth selection adversely affect model performance. To address this, we conduct theoretical analyses to explore a proxy that can balance the modeling errors. As noted by (LeCun et al., 2015), accurate prediction relies on learning the important features of each task. Drawing from (Pearl, 2009), the important features are directly linked to the labels and commonly shared among samples within the same class, e.g., the color of webbed feet or the shape of wings in classifying “ducks”. Ignoring factors such as data sampling errors, the modeling errors directly impact the ability of models to extract important features. For instance, modeling errors may cause underfitting or overfitting, which results in biased learning of important features. Thus, we aim to constrain the model to capture important features of different tasks without changing the model structure to achieve the proxy. Considering the multi-task joint learning mechanism (Finn et al., 2017) of meta-learning, we wonder whether it is possible to capture similar or even identical important features from similar tasks. Consider a simple scenario of two binary classification tasks τ_i and τ_j in the same meta-learning batch, with data variables X_i and X_j , and label variables Y_i and Y_j from $\{\pm 1\}$, each task contains task-shared and task-specific factors (Pearl, 2009), we have:

Theorem 3.1. *Regardless of the correlation between Y_i and Y_j , the classifier for τ_i assigns non-zero weights for task-specific factors of τ_j with importance $\zeta \propto \text{sim}(X_i, X_j)$ achieve better performance, where $\text{sim}(\cdot)$ is the similarity.*

Theorem 3.1 shows that the optimal classifier for a specific task leverages information from other tasks to promote learning. The promotion effect is stronger if the tasks are more similar with the weight $\text{sim}(X_i, X_j)$. Based on this, we propose enforcing task-specific model outputs to be similar on similar tasks, the meta-learning model can obtain optimal classifier and capture effective features. See **Appendix B** for detailed proofs and analyses. **This inspires us to leverage task relations to highlight important features, enhancing the performance of \mathcal{F}_θ across all tasks.**

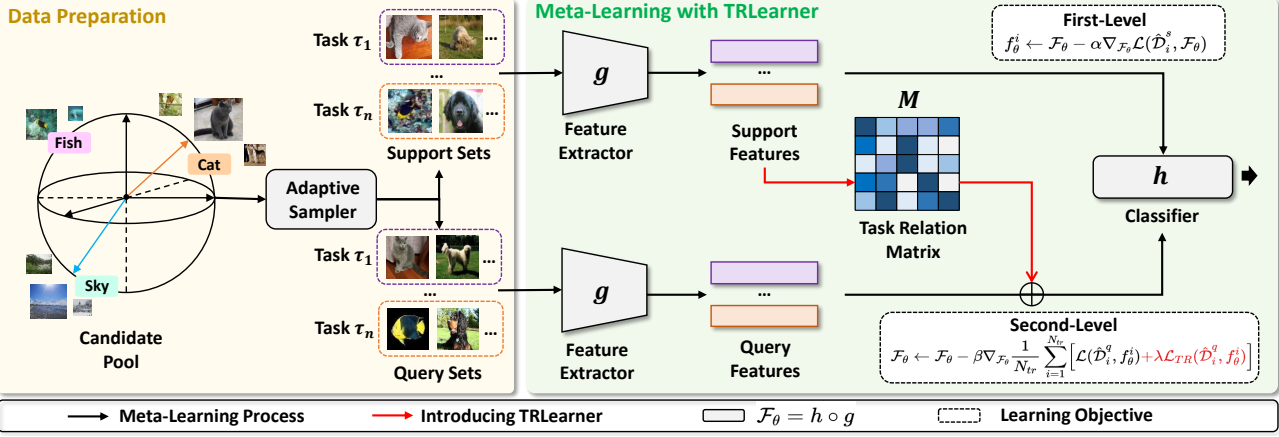


Figure 3. Illustration of meta-learning with TRLearner. TRLearner uses the task relation matrix \mathcal{M} and the regularization term \mathcal{L}_{TR} to calibrate optimization. The black line is for the original meta-learning process, while the red line represents the calibration by TRLearner.

4. Method

Based on this insight, we propose Task Relation Learner (TRLearner), which uses task relation to calibrate meta-learning. Specifically, we first extract the task relation matrix from the sampled task-specific meta-data (**Subsection 4.1**). The elements in this matrix reflect the similarity between tasks. Then, we introduce a relation-aware consistency regularization with the obtained matrix to calibrate meta-learning optimization (**Subsection 4.2**). Based on **Theorem 3.1**, the regularization term constrains the outputs of meta-learning model \mathcal{F}_θ on similar tasks achieve similar performance, enforcing the model focus on important features. Finally, in **Subsection 4.3**, introduce the overall objective of meta-learning with TRLearner. The framework and pseudo-code are shown in **Figure 3** and **Appendix A**.

4.1. Extracting Task Relations

We first discuss how to obtain the task relation matrix $\mathcal{M} = \{m_{ij}\}_{i=1, j \neq i}^{N_{tr}}$ between different tasks. Each element m_{ij} quantifies the similarity between tasks τ_i and τ_j . N_{tr} denotes the number of tasks. Note that directly calculating similarity from all the data within the tasks to obtain \mathcal{M} may cause errors due to sampling randomness and distribution shifts (Wang et al., 2024a). Therefore, we propose using a learnable multi-headed similarity layer to acquire \mathcal{M} .

Specifically, we first obtain meta-data for each task that reflects the discriminative information using an adaptive sampler (Wang et al., 2024a). The higher the sampling scores, the more discriminative the samples are, the greater the sampling probability. We denote the meta-data for task τ_i as: $\hat{\mathcal{D}}_i^s$ for support set and $\hat{\mathcal{D}}_i^q$ for query set. Next, we use a multi-headed layer with parameters \mathcal{W} to obtain task relations \mathcal{M} . Taking task τ_i and task τ_j as examples, we first input the extracted support sets, i.e., $\hat{\mathcal{D}}_i^s$ and $\hat{\mathcal{D}}_j^s$, into the meta-learning model \mathcal{F}_θ . Through the feature extractor

g , we obtain the corresponding task representations $g(\hat{\mathcal{D}}_i^s)$ and $g(\hat{\mathcal{D}}_j^s)$. Then, we calculate their similarity m_{ij} with \mathcal{W} :

$$m_{i,j} = \frac{1}{K} \sum_{k=1}^K \cos(\omega_k \odot g(\hat{\mathcal{D}}_i^s), \omega_k \odot g(\hat{\mathcal{D}}_j^s)), \quad (4)$$

where K denotes the number of heads, \odot denotes the Hadamard product, and $\{\omega_k\}_{k=1}^K$ denotes the learnable vectors of \mathcal{W} which shares the same dimensions as the task representation, e.g., $g(\hat{\mathcal{D}}_i^s)$. It aims to accentuate variations across the different dimensions within the vector space. Note that the initial weights of the matrix are all 1, i.e., $\omega_k = 1$. By calculating the relation between each two tasks in the same batch, we obtain the task relation matrix \mathcal{M} .

4.2. Calibrating Meta-Learning

In this subsection, we illustrate how the relation-aware consistency regularization is designed to enforce the meta-learning model focus on important features. According to **Subsection 3.2**, a well-designed meta-learning model \mathcal{F}_θ should output similar results on similar tasks. Based on this, we propose a relation-aware consistency regularization term \mathcal{L}_{TR} . It constrains the task-specific models on similar tasks to perform similarly based on \mathcal{M} , enforcing \mathcal{F}_θ to learn important features. For task τ_i , it can be expressed as:

$$\mathcal{L}_{TR}(\hat{\mathcal{D}}_i^q, f_\theta^i) = \frac{1}{N_i^q} \sum_{j=1}^{N_i^q} \ell\left(\frac{\sum_{p=1, p \neq i}^{N_{tr}} m_{ip} f_\theta^p(x_{ij})}{\sum_{q=1, q \neq i}^{N_{tr}} m_{iq}}, y_{i,j}\right), \quad (5)$$

where m_{ip} is the strength of the relation between task τ_i and τ_p . $\ell(\cdot)$ is the loss that promotes the alignment of the ground truth with the weighted average prediction obtained from all other task-specific models. Thus, \mathcal{L}_{TR} encourages \mathcal{F}_θ to reinforce the interconnections among task-specific models. Notably, its effectiveness lies in its ability to leverage task relations to emphasize important features—essentially

filtering the task information—and thus maintaining effectiveness even when tasks are highly diverse (Appendix D).

4.3. Overall Objective

In this subsection, we present how to embed TRLearner and how it calibrates the optimization process of meta-learning.

We begin by explaining how we embed TRLearner into meta-learning, i.e., the network structure. We adopt a multi-head neural network architecture consisting of a feature extractor g , a multi-headed similarity layer with weight \mathcal{W} , and a classifier h . The multi-headed layer is for TRLearner, which is used to extract the task relation matrix \mathcal{M} (Eq.4).

Next, we illustrate how TRLearner calibrates the optimization process of meta-learning. Firstly, we input each support set $\hat{\mathcal{D}}_i^s$ into the model \mathcal{F}_θ which outputs task-specific model f_θ^i with one meta-layer. Then, we calculate the task relation matrix via Eq.4 based on these outputs. Next, we update \mathcal{F}_θ by evaluating the output f_θ^i with the relation-aware consistency regularization term \mathcal{L}_{TR} on the each query set $\hat{\mathcal{D}}_i^q$. For the learning objective, the main difference from Eq.3 is adding the regularization term \mathcal{L}_{TR} with the matrix \mathcal{M} :

$$\arg \min_{\mathcal{F}_\theta} \frac{1}{N_{tr}} \sum_{i=1}^{N_{tr}} \left[\mathcal{L}(\hat{\mathcal{D}}_i^q, f_\theta^i) + \lambda \mathcal{L}_{TR}(\hat{\mathcal{D}}_i^q, f_\theta^i) \right], \quad (6)$$

where $\hat{\mathcal{D}}_i^s$ denotes the meta-data. As stated in the fifth paragraph of Subsection 3.1, it can be reformulated as a bi-level optimization process. In the first level, the model \mathcal{F}_θ follows the same objective as Eq.1 but using meta-data:

$$f_\theta^i \leftarrow \mathcal{F}_\theta - \alpha \nabla_{\mathcal{F}_\theta} \mathcal{L}(\hat{\mathcal{D}}_i^s, \mathcal{F}_\theta), \\ \text{where } \mathcal{L}(\hat{\mathcal{D}}_i^s, \mathcal{F}_\theta) = \frac{1}{N_i^s} \sum_{j=1}^{N_i^s} y_{i,j}^s \log \mathcal{F}_\theta(x_{i,j}^s), \quad (7)$$

where α denotes the learning rate. Obtaining task-specific models, TRLearner calculates the task relation matrix via Eq.4. In the second level, we optimize the model \mathcal{F}_θ with the obtained \mathcal{M} and the regularization term \mathcal{L}_{TR} :

$$\mathcal{F}_\theta \leftarrow \mathcal{F}_\theta - \beta \nabla_{\mathcal{F}_\theta} \frac{1}{N_{tr}} \sum_{i=1}^{N_{tr}} \left[\mathcal{L}(\hat{\mathcal{D}}_i^q, f_\theta^i) + \lambda \mathcal{L}_{TR}(\hat{\mathcal{D}}_i^q, f_\theta^i) \right], \\ \text{where } \mathcal{L}(\hat{\mathcal{D}}_i^q, f_\theta^i) = \frac{1}{N_i^q} \sum_{j=1}^{N_i^q} y_{i,j}^q \log f_\theta^i(x_{i,j}^q), \quad (8)$$

where β is the learning rate and λ is the importance weight of \mathcal{L}_{TR} . By doing so, meta-learning can utilize additional task relation information to calibrate the optimization process without changing data or model structure.

5. Theoretical Analysis

In this section, we conduct theoretical analyses to evaluate the effectiveness of TRLearner. We first provide an upper bound on the excess risk, showing that by introducing TRLearner, we can obtain a smaller excess risk (Theorem 5.1).

Next, we show that leveraging the accurate task relations achieves better generalization than previous methods that treat all training tasks equally (Theorem 5.2). The related assumptions and proofs are provided in Appendix B.

First, we provide the maximum limit of excess risk.

Theorem 5.1. *Assume that for every task, the training data \mathcal{D}_i^{tr} contains N_i^{tr} that is approximately greater than or equal to the minimum number of samples found across all tasks, i.e., N_{sh} . If the loss function $\ell(\cdot)$ is Lipschitz continuous concerning its first parameter, then for the test task τ^{te} , the excess risk adheres to the following condition:*

$$\sum_{(x,y) \in \mathcal{D}^{te}} [\ell(\mathcal{F}_\theta^*(x), y) - \ell(\mathcal{F}_\theta(x), y)] \leq \sigma + \sqrt{\frac{\mathcal{R}(\mathcal{H})}{N_{sh} N_{tr} \sigma^k}}, \quad (9)$$

where N_{tr} denotes the number of tasks, while the other symbols, e.g., σ , k , etc., are the same as in Assumption B.1.

It suggests that incorporating task relations can close the distance between training and test risks, resulting in a decrease in the excess risk as the number of training tasks increases.

Next, we prove that obtaining an accurate task relation matrix \mathcal{M} can enhance the OOD generalization of meta-learning. Specifically, we denote the task relation matrix obtained via TRLearner as \mathcal{M} , and the matrix of previous methods as $\tilde{\mathcal{M}}$, where all elements are set to 1. We get:

Theorem 5.2. *Consider the function class \mathcal{H} that satisfies Assumption B.1 and the same conditions as Theorem 5.1, define $r(\mathcal{F}_\theta^*, \mathcal{M})$ as the excess risk with task relation matrix \mathcal{M} , we have $\inf_{\mathcal{F}_\theta^*} \sup_{h \in \mathcal{H}} r(\mathcal{F}_\theta^*, \mathcal{M}) - \inf_{\mathcal{F}_\theta^*} \sup_{h \in \mathcal{H}} r(\mathcal{F}_\theta^*, \tilde{\mathcal{M}}) < 0$.*

Theorem 5.2 shows that introducing \mathcal{M} achieves better generalization compared to $\tilde{\mathcal{M}}$, i.e., having smaller excess risk. Thus, our TRLearner effectively enhances the generalization performance of meta-learning with theoretical support.

6. Experiments

To evaluate the effectiveness of TRLearner, we conduct experiments on (i) regression (Subsection 6.1), (ii) image classification (Subsection 6.2), (iii) drug activity prediction (Subsection 6.3), and (iv) pose prediction (Subsection 6.4). We apply TRLearner to multiple meta-learning methods, e.g., MAML (Finn et al., 2017), MetaSGD (Li et al., 2017), ANIL (Raghu et al., 2019a), and T-NET (Lee & Choi, 2018). For comparison, we consider the regularizers which handle meta-learning, i.e., Meta-Aug (Rajendran et al., 2020), MetaMix (Yao et al., 2021), Dropout-Bins (Jiang et al., 2022) and MetaCRL (Wang et al., 2023), and the SOTA methods proposed for generalization, i.e., Meta-Trans (Bengio et al., 2019), MR-MAML (Yin et al., 2020), iMOL (Wu et al., 2023), OOD-MAML (Jeong & Kim, 2020), and Ro-toGBML (Zhang et al., 2023). We also conduct ablation studies to evaluate how TRLearner works (Subsection 6.5).

Table 1. Performance (MSE) comparison on the Sinusoid and Harmonic regression. The best results are highlighted in **bold**, and TRLearner’s results are highlighted in **orange**.

MODEL	(SIN,5-SHOT)	(SIN,10-SHOT)	(HAR,5-SHOT)	(HAR,10-SHOT)
MR-MAML	0.581 \pm 0.110	0.104 \pm 0.029	0.590 \pm 0.125	0.247 \pm 0.089
META-TRANS	0.577 \pm 0.123	0.097 \pm 0.024	0.576 \pm 0.116	0.231 \pm 0.074
iMOL	0.572 \pm 0.107	0.083 \pm 0.018	0.563 \pm 0.108	0.228 \pm 0.062
OOD-MAML	0.553 \pm 0.112	0.076 \pm 0.021	0.552 \pm 0.103	0.224 \pm 0.058
ROTOGBML	0.546 \pm 0.104	0.061 \pm 0.012	0.539 \pm 0.101	0.216 \pm 0.043
MAML	0.593 \pm 0.120	0.166 \pm 0.061	0.622 \pm 0.132	0.256 \pm 0.099
MAML+META-AUG	0.531 \pm 0.118	0.103 \pm 0.031	0.596 \pm 0.127	0.247 \pm 0.094
MAML+METAMIX	0.476 \pm 0.109	0.085 \pm 0.024	0.576 \pm 0.114	0.236 \pm 0.097
MAML+DROPOUT-BINS	0.452 \pm 0.081	0.062 \pm 0.017	0.561 \pm 0.109	0.235 \pm 0.056
MAML+METACRL	0.440 \pm 0.079	0.054 \pm 0.018	0.548 \pm 0.103	0.211 \pm 0.071
MAML+TRLERNER	0.400 \pm 0.064	0.052 \pm 0.016	0.539 \pm 0.101	0.204 \pm 0.037
ANIL	0.541 \pm 0.118	0.103 \pm 0.032	0.573 \pm 0.124	0.205 \pm 0.072
ANIL+META-AUG	0.536 \pm 0.115	0.097 \pm 0.026	0.561 \pm 0.119	0.197 \pm 0.064
ANIL+METAMIX	0.514 \pm 0.106	0.083 \pm 0.022	0.554 \pm 0.113	0.184 \pm 0.053
ANIL+DROPOUT-BINS	0.487 \pm 0.110	0.088 \pm 0.025	0.541 \pm 0.104	0.179 \pm 0.035
ANIL+METACRL	0.468 \pm 0.094	0.081 \pm 0.019	0.533 \pm 0.083	0.153 \pm 0.031
ANIL+TRLERNER	0.471 \pm 0.081	0.075 \pm 0.023	0.517 \pm 0.074	0.134 \pm 0.028
METASGD	0.577 \pm 0.126	0.152 \pm 0.044	0.612 \pm 0.138	0.248 \pm 0.076
METASGD+META-AUG	0.524 \pm 0.122	0.138 \pm 0.027	0.608 \pm 0.126	0.231 \pm 0.069
METASGD+METAMIX	0.468 \pm 0.118	0.072 \pm 0.023	0.595 \pm 0.117	0.226 \pm 0.062
METASGD+DROPOUT-BINS	0.435 \pm 0.089	0.040 \pm 0.011	0.578 \pm 0.109	0.213 \pm 0.057
METASGD+METACRL	0.408 \pm 0.071	0.038 \pm 0.010	0.551 \pm 0.104	0.195 \pm 0.042
METASGD+TRLERNER	0.391 \pm 0.057	0.024 \pm 0.008	0.532 \pm 0.101	0.176 \pm 0.027
T-NET	0.564 \pm 0.128	0.111 \pm 0.042	0.597 \pm 0.135	0.214 \pm 0.078
T-NET+META-AUG	0.521 \pm 0.124	0.105 \pm 0.031	0.584 \pm 0.122	0.207 \pm 0.063
T-NET+METAMIX	0.498 \pm 0.113	0.094 \pm 0.025	0.576 \pm 0.119	0.183 \pm 0.054
T-NET+DROPOUT-BINS	0.470 \pm 0.091	0.077 \pm 0.028	0.559 \pm 0.113	0.174 \pm 0.035
T-NET+METACRL	0.462 \pm 0.078	0.071 \pm 0.019	0.554 \pm 0.112	0.158 \pm 0.024
T-NET+TRLERNER	0.443 \pm 0.058	0.066 \pm 0.012	0.543 \pm 0.102	0.144 \pm 0.013

All results are averaged from five runs on NVIDIA V100 GPUs. More details are provided in [Appendices E-H](#).

6.1. Performance on Regression

Experimental Setup. We select (i) Sinusoid dataset ([Jiang et al., 2022](#)) with 480 tasks from $A \sin w \cdot x + b + \epsilon$, where $A \in [0.1, 5.0]$, $w \in [0.5, 2.0]$, and $b \in [0, 2\pi]$. Gaussian noise with a mean (μ) of 0 and a standard deviation (ϵ) of 0.3 is added; and (ii) Harmonic dataset ([Wang et al., 2024a](#)) with 480 tasks from a sum of two sine waves with $f(x) = a_1 \sin(\omega x + b_1) + a_2 \sin(2\omega x + b_2)$, where $y \sim \mathcal{N}(f(x), \sigma_y^2)$ where $\mathcal{U}(5, 7)$, (b_1, b_2) from $\mathcal{U}(0, 2\pi)^2$, and (a_1, a_2) from $\mathcal{N}(0, 1)^2$. The metric is Mean Squared Error (MSE).

Results. As shown in [Table 1](#), we can observe that (i) TR-Learner achieves better results than the SOTA baselines, with average MSE reduced by 0.028 and 0.021; (ii) TR-Learner also shows significant improvements in all meta-learning baselines, with MSE reduced by more than 0.1. These results demonstrate the superiority of TRLearner.

6.2. Performance on Image Classification

Experimental Setup. We select two image classification environments, i.e., standard and cross-domain few-shot learning (SFSL and CFSL), with four benchmark datasets, i.e., miniImagenet ([Vinyals et al., 2016](#)), Omniglot ([Lake et al., 2019](#)), CUB ([Welinder et al., 2010](#)), and Places ([Zhou et al., 2017](#)). The evaluation metric is the average accuracy.

Results. From the SFSL and CFSL results in [Table 2](#), we can observe that: (i) In SFSL, TRLearner achieves stable performance improvement and surpasses other comparison baselines; (ii) In CFSL, TRLearner still surpasses the

Table 2. Performance (accuracy \pm 95% confidence interval) of image classification on SFSL, i.e., (20-way 1-shot) Omniglot and (5-way 1-shot) miniImagenet, and CFSL settings, i.e., miniImagenet \rightarrow CUB and miniImagenet \rightarrow Places.

MODEL	OMNIGLOT	MINIIMAGENET	\rightarrow CUB	\rightarrow PLACES
MR-MAML	89.28 \pm 0.59	35.01 \pm 1.60	35.76 \pm 1.27	31.23 \pm 0.48
META-TRANS	87.39 \pm 0.51	35.19 \pm 1.58	36.21 \pm 1.36	31.97 \pm 0.52
iMOL	92.89 \pm 0.44	36.27 \pm 1.54	37.14 \pm 1.17	32.44 \pm 0.65
OOD-MAML	93.01 \pm 0.50	37.43 \pm 1.47	39.62 \pm 1.34	35.52 \pm 0.69
ROTOGBML	92.77 \pm 0.69	39.32 \pm 1.62	41.27 \pm 1.24	35.32 \pm 0.58
MAML	87.15 \pm 0.61	33.16 \pm 1.70	33.62 \pm 1.18	29.84 \pm 0.56
MAML+META-AUG	89.77 \pm 0.62	34.76 \pm 1.52	35.07 \pm 1.24	30.57 \pm 0.63
MAML+METAMIX	91.97 \pm 0.51	38.97 \pm 1.81	36.29 \pm 1.37	31.76 \pm 0.49
MAML+DROPOUT-BINS	92.89 \pm 0.46	39.66 \pm 1.74	37.41 \pm 1.12	33.69 \pm 0.78
MAML+METACRL	93.00 \pm 0.42	41.55 \pm 1.76	38.16 \pm 1.27	35.41 \pm 0.53
MAML+TRLERNER	94.23 \pm 0.56	42.86 \pm 1.83	40.54 \pm 1.26	36.12 \pm 0.64
ANIL	89.17 \pm 0.56	34.96 \pm 1.71	35.74 \pm 1.16	31.64 \pm 0.57
ANIL+META-AUG	90.46 \pm 0.47	35.44 \pm 1.73	36.32 \pm 1.28	32.58 \pm 0.64
ANIL+METAMIX	92.88 \pm 0.51	37.82 \pm 1.75	36.89 \pm 1.34	33.72 \pm 0.61
ANIL+DROPOUT-BINS	92.82 \pm 0.49	38.09 \pm 1.76	38.24 \pm 1.17	33.94 \pm 0.66
ANIL+METACRL	92.91 \pm 0.52	38.55 \pm 1.81	39.68 \pm 1.32	34.47 \pm 0.52
ANIL+TRLERNER	93.24 \pm 0.48	38.73 \pm 1.84	41.96 \pm 1.24	35.68 \pm 0.61
METASGD	87.81 \pm 0.61	33.97 \pm 0.92	33.65 \pm 1.13	29.83 \pm 0.66
METASGD+META-AUG	88.56 \pm 0.57	35.76 \pm 0.91	34.73 \pm 1.32	31.49 \pm 0.54
METASGD+METAMIX	93.44 \pm 0.45	40.28 \pm 0.96	35.26 \pm 1.21	32.76 \pm 0.59
METASGD+DROPOUT-BINS	93.93 \pm 0.40	40.31 \pm 0.96	37.49 \pm 1.37	33.21 \pm 0.67
METASGD+METACRL	94.12 \pm 0.43	41.22 \pm 0.93	38.61 \pm 1.25	35.83 \pm 0.63
METASGD+TRLERNER	94.57 \pm 0.49	41.64 \pm 0.94	39.58 \pm 1.13	36.42 \pm 0.54
T-NET	87.66 \pm 0.59	33.69 \pm 1.72	34.82 \pm 1.17	28.77 \pm 0.48
T-NET+META-AUG	91.29 \pm 0.53	35.24 \pm 1.74	35.42 \pm 1.28	30.54 \pm 0.57
T-NET+METAMIX	93.16 \pm 0.48	39.18 \pm 1.73	37.22 \pm 1.37	31.28 \pm 0.61
T-NET+DROPOUT-BINS	93.54 \pm 0.49	39.06 \pm 1.72	37.49 \pm 1.14	32.37 \pm 0.55
T-NET+METACRL	93.81 \pm 0.52	40.08 \pm 1.74	38.47 \pm 1.36	33.69 \pm 0.48
T-NET+TRLERNER	94.33 \pm 0.54	40.31 \pm 1.75	40.64 \pm 1.29	34.76 \pm 0.62

SOTA baseline. Combined with the trade-off performance in [Appendix H](#), TRLearner achieves the best generalization improvement under the condition of lower computational cost. This further proves the superiority of TRLearner.

6.3. Performance on Drug Activity Prediction

Experimental Setup. We assess TRLearner for drug activity prediction using the pQSAR dataset ([Martin et al., 2019](#)), which forecasts compound activity on proteins with 4,276 tasks. Following ([Martin et al., 2019](#); [Yao et al., 2021](#)), we divide the tasks into four groups but conduct the “Group 5” that contains tasks from the other four groups for average evaluation. The evaluation metric is the squared Pearson correlation coefficient (R^2), indicating the correlation between predictions and ground-truth. We report the mean and median R^2 and the count of R^2 exceeding 0.3.

Results. As shown in [Table 3](#), TRLearner achieves comparable performance to the SOTA baselines. Considering that drug activity prediction is a more complex task ([Martin et al., 2019](#)), TRLearner not only narrows the gap between the R^2 Mean and R^2 Median scores but also achieves an improvement in the reliability index $R^2 > 0.3$, demonstrating its superior performance in complex scenarios.

6.4. Performance on Pose Prediction

Experimental Setup. We use the Pascal 3D dataset ([Xiang et al., 2014](#)) as benchmark dataset for pose prediction. We randomly select 50 objects for training and 15 objects for testing. The evaluation metric employed here is MSE.

Results. As shown in [Table 4](#), TRLearner achieves SOTA

Table 3. Performance on drug activity prediction. “Mean”, “Med.”, “ > 0.3 ” are the mean, the median value of R^2 , and $R^2 > 0.3$.

MODEL	GROUP 1			GROUP 2			GROUP 3			GROUP 4			GROUP 5 (AVERAGE)		
	MEAN	MED.	> 0.3	MEAN	MED.	> 0.3									
MAML	0.371	0.315	52	0.321	0.254	43	0.318	0.239	44	0.348	0.281	47	0.341	0.260	45
MAML+DROPOUT-BINS	0.410	0.376	60	0.355	0.257	48	0.320	0.275	46	0.370	0.337	56	0.380	0.314	52
MAML+METACRL	0.413	0.378	61	0.360	0.261	50	0.334	0.282	51	0.375	0.341	59	0.371	0.316	56
MAML+TRLEARNER	0.418	0.380	62	0.366	0.263	52	0.342	0.285	52	0.379	0.339	59	0.378	0.319	56
ANIL	0.355	0.296	50	0.318	0.297	49	0.304	0.247	46	0.338	0.301	50	0.330	0.284	48
ANIL+METAMIX	0.347	0.292	49	0.302	0.258	45	0.301	0.282	47	0.348	0.303	51	0.327	0.284	48
ANIL+DROPOUT-BINS	0.394	0.321	53	0.338	0.271	48	0.312	0.284	46	0.368	0.297	50	0.350	0.271	49
ANIL+TRLEARNER	0.402	0.341	57	0.347	0.276	49	0.320	0.296	48	0.374	0.306	53	0.364	0.304	51

 Table 4. Performance (MSE \pm 95% confidence interval) comparison on pose prediction. The best results are highlighted in **bold**.

MODEL	MSE WITH 10-SHOT	MSE WITH 15-SHOT
MAML	3.113 ± 0.241	2.496 ± 0.182
MAML + METAMIX	2.429 ± 0.198	1.987 ± 0.151
MAML + DROPOUT-BINS	2.396 ± 0.209	1.961 ± 0.134
MAML + METACRL	2.355 ± 0.200	1.931 ± 0.134
MAML + TRLEARNER	2.334 ± 0.216	1.875 ± 0.132
METASGD	2.811 ± 0.239	2.017 ± 0.182
METASGD + METAMIX	2.388 ± 0.204	1.952 ± 0.134
METASGD + DROPOUT-BINS	2.369 ± 0.217	1.927 ± 0.120
METASGD + METACRL	2.362 ± 0.196	1.920 ± 0.191
METASGD + TRLEARNER	2.357 ± 0.188	1.893 ± 0.176
T-NET	2.841 ± 0.177	2.712 ± 0.225
T-NET + METAMIX	2.562 ± 0.280	2.410 ± 0.192
T-NET + DROPOUT-BINS	2.487 ± 0.212	2.402 ± 0.178
T-NET + METACRL	2.481 ± 0.274	2.400 ± 0.171
T-NET + TRLEARNER	2.476 ± 0.248	2.398 ± 0.167

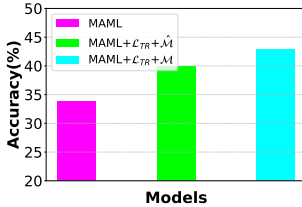
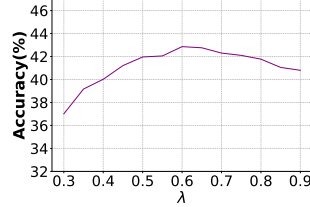

 Figure 4. Effect of regularization \mathcal{L}_{TR} on miniImagenet.


Figure 5. Parameter sensitivity on miniImagenet.

performance without additional data. Studies (Yao et al., 2021) have shown that augmentations in pose prediction may achieve better results, but TRLearner can achieve similar improvements, further proving its effectiveness.

6.5. Ablation Study

In this subsection, we provide the results of the ablation studies, with more experiments in Appendix H.

Effect of \mathcal{L}_{TR} . We evaluate the performance of MAML before and after introducing \mathcal{L}_{TR} on miniImagenet, where \mathcal{L}_{TR} is the core of TRLearner. We also evaluate the adaptive learning method of the task relation matrix \mathcal{M} by replacing it with a fixed calculation, i.e., directly calculating the similarity between the sampled meta-data ($\hat{\mathcal{M}}$). As shown in Figure 4, (i) the model with \mathcal{L}_{TR} has significant improvement and negligible computational overhead; (ii) the adaptively learned \mathcal{M} is more accurate than the fixed calculation. This proves the effectiveness of TRLearner.

Parameter Sensitivity. We determine the hyperparameters λ of the regularization term \mathcal{L}_{TR} by evaluating the

impact of different values of λ on the performance of MAML+TRLearner with the range [0.3, 0.8]. The results in Figure 5 show that (i) $\lambda = 0.6$ is the best (also our setting), and (ii) TRLearner has minimal variation in accuracy, indicating that hyperparameter tuning is easy in practice.

7. Related Work

Meta-Learning seeks to acquire general knowledge from various tasks and then apply it to new tasks. Typical methods can be divided into two categories: optimization-based (Finn et al., 2017; Nichol & Schulman, 2018) and metric-based methods (Shell et al., 2017; Sung et al., 2018). They both rely on bi-level optimization to learn general knowledge, resulting in remarkable performance on new tasks. Despite its adaptability to various scenarios (Sun, 2023; Li et al., 2018; Yao et al., 2021; Wang et al., 2024b), meta-learning still may face over-fitting or under-fitting issues on different tasks. Some works (Jamal & Qi, 2019; Lee et al., 2020; Yao et al., 2021) proposed addressing these issues by maintaining network overparameterization while enhancing data or its information content. However, these methods rely on augmentation strategies and sufficient training which highly increases the computational overhead. They focus on changing data but ignore the impact of the more essential “learning to learn” strategy of meta-learning, where exists a gap between theoretical understanding and practical implementation. In contrast, we rethink the learning paradigm to explore what causes errors and how to eliminate them. More details about related works are shown in Appendix I.

8. Conclusion

In this paper, we rethink meta-learning from the “learning” lens to unify the theoretical understanding and practical implementation. Through empirical and theoretical analyses, we find that (i) existing meta-learning relying on one meta-layer faces the risks of overfitting and underfitting according to tasks; and (ii) the models adapted to different tasks promote each other where the promotion is related to task relations. Based on these results, we propose TRLearner, a plug-and-play method that uses task relation to calibrate meta-learning optimization. Extensive theoretical and empirical analyses demonstrate its effectiveness.

Impact Statement

This paper presents work whose goal is to advance the field of Machine Learning and Meta-Learning. There are many potential societal consequences of our work, none of which we feel must be specifically highlighted here.

References

Anderson, N. H. Cross-task validation of functional measurement. *Perception & Psychophysics*, 12(5):389–395, 1972.

Appel, T., Gerjets, P., Hoffman, S., Moeller, K., Ninaus, M., Schärling, C., Sevcenko, N., Wortha, F., and Kasneci, E. Cross-task and cross-participant classification of cognitive load in an emergency simulation game. *IEEE Transactions on Affective Computing*, 2021.

Barrett, D. G. and Dherin, B. Implicit gradient regularization. *arXiv preprint arXiv:2009.11162*, 2020.

Baxter, J. A bayesian/information theoretic model of learning to learn via multiple task sampling. *Machine learning*, 28:7–39, 1997.

Bengio, Y., Deleu, T., Rahaman, N., Ke, R., Lachapelle, S., Bilaniuk, O., Goyal, A., and Pal, C. A meta-transfer objective for learning to disentangle causal mechanisms. *arXiv preprint arXiv:1901.10912*, 2019.

Bohdal, O., Yang, Y., and Hospedales, T. Meta-calibration: Learning of model calibration using differentiable expected calibration error. *arXiv preprint arXiv:2106.09613*, 2021.

Boutilier, C., Hsu, C.-w., Kveton, B., Mladenov, M., Szepesvari, C., and Zaheer, M. Differentiable meta-learning of bandit policies. *Advances in Neural Information Processing Systems*, 33:2122–2134, 2020.

Chen, W.-Y., Liu, Y.-C., Kira, Z., Wang, Y.-C. F., and Huang, J.-B. A closer look at few-shot classification. *arXiv preprint arXiv:1904.04232*, 2019.

Chen, Y., Guan, C., Wei, Z., Wang, X., and Zhu, W. Metadelta: A meta-learning system for few-shot image classification. In *AAAI Workshop on Meta-Learning and MetaDL Challenge*, pp. 17–28. PMLR, 2021.

Choe, S., Mehta, S. V., Ahn, H., Neiswanger, W., Xie, P., Strubell, E., and Xing, E. Making scalable meta learning practical. *Advances in neural information processing systems*, 36, 2024.

Daubechies, I., DeVore, R., Foucart, S., Hanin, B., and Petrova, G. Nonlinear approximation and (deep) relu networks. *Constructive Approximation*, 55(1):127–172, 2022.

Finn, C., Abbeel, P., and Levine, S. Model-agnostic meta-learning for fast adaptation of deep networks. In *International conference on machine learning*, pp. 1126–1135. PMLR, 2017.

Flennerhag, S., Rusu, A. A., Pascanu, R., Visin, F., Yin, H., and Hadsell, R. Meta-learning with warped gradient descent. *arXiv preprint arXiv:1909.00025*, 2019.

Flennerhag, S., Schroecker, Y., Zahavy, T., van Hasselt, H., Silver, D., and Singh, S. Bootstrapped meta-learning. *arXiv preprint arXiv:2109.04504*, 2021.

Gaulton, A., Bellis, L. J., Bento, A. P., Chambers, J., Davies, M., Hersey, A., Light, Y., McGlinchey, S., Michalovich, D., Al-Lazikani, B., et al. ChEMBL: a large-scale bioactivity database for drug discovery. *Nucleic acids research*, 40(D1):D1100–D1107, 2012.

Haarhoff, P. and Buys, J. A new method for the optimization of a nonlinear function subject to nonlinear constraints. *The Computer Journal*, 13(2):178–184, 1970.

Hospedales, T., Antoniou, A., Micaelli, P., and Storkey, A. Meta-learning in neural networks: A survey. *IEEE transactions on pattern analysis and machine intelligence*, 44(9):5149–5169, 2021.

Iscen, A., Araujo, A., Gong, B., and Schmid, C. Class-balanced distillation for long-tailed visual recognition. *arXiv preprint arXiv:2104.05279*, 2021.

Jamal, M. A. and Qi, G.-J. Task agnostic meta-learning for few-shot learning. In *Proceedings of the IEEE/CVF Conference on Computer Vision and Pattern Recognition*, pp. 11719–11727, 2019.

Jeong, T. and Kim, H. Ood-maml: Meta-learning for few-shot out-of-distribution detection and classification. *Advances in Neural Information Processing Systems*, 33: 3907–3916, 2020.

Jiang, Y., Chen, Z., Kuang, K., Yuan, L., Ye, X., Wang, Z., Wu, F., and Wei, Y. The role of deconfounding in meta-learning. In *International Conference on Machine Learning*, pp. 10161–10176. PMLR, 2022.

Khadka, R., Jha, D., Hicks, S., Thambawita, V., Riegler, M. A., Ali, S., and Halvorsen, P. Meta-learning with implicit gradients in a few-shot setting for medical image segmentation. *Computers in Biology and Medicine*, 143: 105227, 2022.

Kim, S., Purdie, T. G., and McIntosh, C. Cross-task attention network: Improving multi-task learning for medical imaging applications. In *International Conference on Medical Image Computing and Computer-Assisted Intervention*, pp. 119–128. Springer, 2023.

Kung, P.-N., Yin, F., Wu, D., Chang, K.-W., and Peng, N. Active instruction tuning: Improving cross-task generalization by training on prompt sensitive tasks. *arXiv preprint arXiv:2311.00288*, 2023.

Lacoste, A., Oreshkin, B., Chung, W., Boquet, T., Ros-tamzadeh, N., and Krueger, D. Uncertainty in multitask transfer learning. *arXiv preprint arXiv:1806.07528*, 2018.

Lake, B. M., Salakhutdinov, R., and Tenenbaum, J. B. The omniglot challenge: a 3-year progress report. *Current Opinion in Behavioral Sciences*, 29:97–104, 2019.

LeCun, Y., Bengio, Y., and Hinton, G. Deep learning. *nature*, 521(7553):436–444, 2015.

Lee, H. B., Nam, T., Yang, E., and Hwang, S. J. Meta dropout: Learning to perturb latent features for generalization. 2020.

Lee, J., Tack, J., Lee, N., and Shin, J. Meta-learning sparse implicit neural representations. *Advances in Neural Information Processing Systems*, 34:11769–11780, 2021.

Lee, Y. and Choi, S. Gradient-based meta-learning with learned layerwise metric and subspace. In *International Conference on Machine Learning*, pp. 2927–2936. PMLR, 2018.

Li, D., Yang, Y., Song, Y.-Z., and Hospedales, T. Learning to generalize: Meta-learning for domain generalization. In *Proceedings of the AAAI conference on artificial intelligence*, volume 32, 2018.

Li, T., Wang, L., and Wu, G. Self supervision to distillation for long-tailed visual recognition. In *Proceedings of the IEEE/CVF international conference on computer vision*, pp. 630–639, 2021.

Li, X., Deng, W., Li, S., and Li, Y. Compound expression recognition in-the-wild with au-assisted meta multi-task learning. In *Proceedings of the IEEE/CVF Conference on Computer Vision and Pattern Recognition*, pp. 5734–5743, 2023.

Li, Z., Zhou, F., Chen, F., and Li, H. Meta-sgd: Learning to learn quickly for few-shot learning. *arXiv preprint arXiv:1707.09835*, 2017.

Lin, M., Li, W., Li, D., Chen, Y., Li, G., and Lu, S. Multi-domain generalized graph meta learning. In *Proceedings of the AAAI Conference on Artificial Intelligence*, volume 37, pp. 4479–4487, 2023.

Liu, R., Bai, F., Du, Y., and Yang, Y. Meta-reward-net: Implicitly differentiable reward learning for preference-based reinforcement learning. *Advances in Neural Information Processing Systems*, 35:22270–22284, 2022.

Martin, E. J., Polyakov, V. R., Zhu, X.-W., Tian, L., Mukherjee, P., and Liu, X. All-assay-max2 pqsar: activity predictions as accurate as four-concentration ic50s for 8558 novartis assays. *Journal of chemical information and modeling*, 59(10):4450–4459, 2019.

Maurer, A., Pontil, M., and Romera-Paredes, B. The benefit of multitask representation learning. *Journal of Machine Learning Research*, 17(81):1–32, 2016.

Mohri, M. Foundations of machine learning, 2018.

Nichol, A. and Schulman, J. Reptile: a scalable metalearning algorithm. *arXiv preprint arXiv:1803.02999*, 2(3):4, 2018.

Nichol, A., Achiam, J., and Schulman, J. On first-order meta-learning algorithms. *arXiv preprint arXiv:1803.02999*, 2018.

Pearl, J. *Causality*. Cambridge university press, 2009.

Pinkus, A. Approximation theory of the mlp model in neural networks. *Acta numerica*, 8:143–195, 1999.

Raghu, A., Raghu, M., Bengio, S., and Vinyals, O. Rapid learning or feature reuse? towards understanding the effectiveness of maml. *arXiv preprint arXiv:1909.09157*, 2019a.

Raghu, A., Raghu, M., Bengio, S., and Vinyals, O. Rapid learning or feature reuse? towards understanding the effectiveness of maml. *arXiv preprint arXiv:1909.09157*, 2019b.

Rajendran, J., Irpan, A., and Jang, E. Meta-learning requires meta-augmentation. *NeurIPS*, 2020.

Rajeswaran, A., Finn, C., Kakade, S. M., and Levine, S. Meta-learning with implicit gradients. *Advances in neural information processing systems*, 32, 2019.

Sauer, A., Asaadi, S., and Küch, F. Knowledge distillation meets few-shot learning: An approach for few-shot intent classification within and across domains. In *Proceedings of the 4th Workshop on NLP for Conversational AI*, pp. 108–119, 2022.

Schrum, M. L., Hedlund-Botti, E., Moorman, N., and Gombolay, M. C. Mind meld: Personalized meta-learning for robot-centric imitation learning. In *2022 17th ACM/IEEE International Conference on Human-Robot Interaction (HRI)*, pp. 157–165. IEEE, 2022.

Schwartz, J. T. *Nonlinear functional analysis*, volume 4. CRC Press, 1969.

Snell, J., Swersky, K., and Zemel, R. Prototypical networks for few-shot learning. *Advances in neural information processing systems*, 30, 2017.

Standley, T., Zamir, A., Chen, D., Guibas, L., Malik, J., and Savarese, S. Which tasks should be learned together in multi-task learning? In *International conference on machine learning*, pp. 9120–9132. PMLR, 2020.

Sun, Y. Meta learning in decentralized neural networks: towards more general ai. In *Proceedings of the AAAI Conference on Artificial Intelligence*, volume 37, pp. 16137–16138, 2023.

Sung, F., Yang, Y., Zhang, L., Xiang, T., Torr, P. H., and Hospedales, T. M. Learning to compare: Relation network for few-shot learning. In *Proceedings of the IEEE conference on computer vision and pattern recognition*, pp. 1199–1208, 2018.

Taud, H. and Mas, J.-F. Multilayer perceptron (mlp). *Geomatic approaches for modeling land change scenarios*, pp. 451–455, 2018.

Triantafillou, E., Zhu, T., Dumoulin, V., Lamblin, P., Evcı, U., Xu, K., Goroshin, R., Gelada, C., Swersky, K., Mazzagol, P.-A., et al. Meta-dataset: A dataset of datasets for learning to learn from few examples. *arXiv preprint arXiv:1903.03096*, 2019.

Verma, V. K., Brahma, D., and Rai, P. Meta-learning for generalized zero-shot learning. In *Proceedings of the AAAI conference on artificial intelligence*, volume 34, pp. 6062–6069, 2020.

Vinyals, O., Blundell, C., Lillicrap, T., Wierstra, D., et al. Matching networks for one shot learning. *Advances in neural information processing systems*, 29, 2016.

Wang, J., Qiang, W., Ren, Y., Song, Z., Zhang, J., and Zheng, C. Hacking task confounder in meta-learning. *arXiv preprint arXiv:2312.05771*, 2023.

Wang, J., Qiang, W., Su, X., Zheng, C., Sun, F., and Xiong, H. Towards task sampler learning for meta-learning. *International Journal of Computer Vision*, pp. 1–31, 2024a.

Wang, J., Tian, Y., Yang, Y., Chen, X., Zheng, C., and Qiang, W. Meta-auxiliary learning for micro-expression recognition. *arXiv preprint arXiv:2404.12024*, 2024b.

Watrous, R. L. *Learning algorithms for connectionist networks: Applied gradient methods of nonlinear optimization*. University of Pennsylvania, Department of Computer and Information Science, 1988.

Welinder, P., Branson, S., Mita, T., Wah, C., Schroff, F., Belongie, S., and Perona, P. Caltech-ucsd birds 200. 2010.

Wilder, B., Horvitz, E., and Kamar, E. Learning to complement humans. *arXiv preprint arXiv:2005.00582*, 2020.

Wu, X., Lu, J., Fang, Z., and Zhang, G. Meta ood learning for continuously adaptive ood detection. In *Proceedings of the IEEE/CVF International Conference on Computer Vision*, pp. 19353–19364, 2023.

Xiang, Y., Mottaghi, R., and Savarese, S. Beyond pascal: A benchmark for 3d object detection in the wild. In *IEEE winter conference on applications of computer vision*, pp. 75–82. IEEE, 2014.

Yao, H., Huang, L.-K., Zhang, L., Wei, Y., Tian, L., Zou, J., Huang, J., et al. Improving generalization in meta-learning via task augmentation. In *International conference on machine learning*, pp. 11887–11897. PMLR, 2021.

Yin, M., Tucker, G., Zhou, M., Levine, S., and Finn, C. Meta-learning without memorization. *ICLR*, 2020.

Zhang, B., Luo, C., Yu, D., Li, X., Lin, H., Ye, Y., and Zhang, B. Metadiff: Meta-learning with conditional diffusion for few-shot learning. In *Proceedings of the AAAI Conference on Artificial Intelligence*, volume 38, pp. 16687–16695, 2024.

Zhang, M., Zhuang, Z., Wang, Z., Wang, D., and Li, W. Rotogbml: Towards out-of-distribution generalization for gradient-based meta-learning. *arXiv preprint arXiv:2303.06679*, 2023.

Zhao, Q., Jiang, C., Hu, W., Zhang, F., and Liu, J. Mdcs: More diverse experts with consistency self-distillation for long-tailed recognition. In *Proceedings of the IEEE/CVF International Conference on Computer Vision*, pp. 11597–11608, 2023.

Zheng, W., Yan, L., Gou, C., and Wang, F.-Y. Knowledge is power: Hierarchical-knowledge embedded meta-learning for visual reasoning in artistic domains. In *Proceedings of the 27th ACM SIGKDD Conference on Knowledge Discovery & Data Mining*, pp. 2360–2368, 2021.

Zhou, B., Lapedriza, A., Khosla, A., Oliva, A., and Torralba, A. Places: A 10 million image database for scene recognition. *IEEE transactions on pattern analysis and machine intelligence*, 40(6):1452–1464, 2017.

Appendix

The appendix provides supplementary information and additional details that support the primary discoveries and methodologies proposed in this paper. It is organized into several sections:

- Appendix [A](#) encompasses the pseudo-code of meta-learning with TRLearner.
- Appendix [B](#) contains the proofs of the presented theorems.
- Appendix [C](#) provides the details and further analysis about the “learning” lens of meta-learning.
- Appendix [D](#) provide more discussion about the effectiveness of TRLearner, e.g., with highly diverse tasks.
- Appendix [E](#) provides details for all datasets used in the experiments.
- Appendix [F](#) provides details for the baselines used in the experiments.
- Appendix [G](#) presents the implementation and architecture of our method, aiding in faithful reproduction.
- Appendix [H](#) provides additional experiments, full results, and experimental details of the comparison experiments that were omitted in the main text due to page limitations.
- Appendix [I](#) discusses the uniqueness of this work, e.g., comparison with other fields that involve task information.

Note that before we illustrate the details and analysis, we provide a brief summary of all the experiments conducted in this paper, as shown in Table 5.

Table 5. Illustration of the experiments conducted in this work. All experimental results are obtained after five rounds of experiments.

Experiments	Location	Results
Motivating experiments	Section 2 and Appendix H.1	Figure 2, Figure 6, and Figure 7
Performance on regression problems with two benchmark datasets	Section 6.1	Table 1
Performance on image classification with two settings, i.e., standard few-shot learning (miniImagenet and Omnistill) and cross-domain few-shot learning (miniImagenet → CUB and Places)	Section 6.2 and Appendix H.2	Table 2 and Table 6
Performance on drug activity prediction (pQSAR)	Section 6.3 and Appendix H.2	Table 3 and Table 7
Experiment on pose prediction (Pascal 3D)	Section 6.4 and Appendix H.2	Table 4 and Table 8
Ablation Study-Effect of \mathcal{L}_{TR}	Section 6.5	Figure 4
Ablation Study-Parameter Sensitivity	Section 6.5	Figure 5
Results Together with Other Regularizers	Appendix H.3	Table 9 and Table 10
Trade-off Performance Comparison	Appendix H.4	Figure 8
OOD Generalization Performance Comparison	Appendix H.5	Table 11
Task Relation Visualization	Appendix H.6	Figure 9
Performance under different meta-layer	Appendix H.7	Figure 10

A. Pseudo-code

The pseudocode of the meta-learning process with our proposed TRLearner is shown in Algorithm 1. TRLearner is a plug-and-play method that aims to improve generalization by calibrating the meta-learning optimization process based on task relations. Specifically, it first extracts task relations from the sampled task-specific meta-data, obtaining the task relation matrix. Then, it uses the task relation matrix to constrain the optimization of the meta-learning model, i.e., introducing relation-aware consistency regularization term to the second-level meta-learning, obtaining a better meta-learning model that performs well on all task adaptations.

Algorithm 1 Meta-Learning with TRLearner

Input: Task distribution $p(\mathcal{T})$; Randomly initialize meta-learning model f_θ with a feature extractor g and multi-heads h ; Initialize task relation matrix $\mathcal{M} = \mathbb{I}^{N_{tr} \times N_{tr}}$

Parameter: Number of tasks for one batch N_{tr} ; Learning rates α and β for the learning of f_θ ; Loss weight λ for the relation-aware consistency regularization term

Output: Meta-learning model \mathcal{F}_θ

```

1: while not coverage do
2:   Sample tasks  $\tau \sim \{\tau_i\}_{i=1}^{N_{tr}}$  from  $p(\mathcal{T})$  via the adaptive task sampler ▷ Task Construction
3:   for all  $\tau_i$  do
4:     Obtain the support set  $\mathcal{D}_i^s = \{(x_{i,j}^s, y_{i,j}^s)\}_{j=1}^{N_i^s}$  for task  $\tau_i$ 
5:     Obtain the query set  $\mathcal{D}_i^q = \{(x_{i,j}^q, y_{i,j}^q)\}_{j=1}^{N_i^q}$  for task  $\tau_i$ 
6:     Update task relation matrix  $\mathcal{M} = \{m_{ij}\}_{i=1, j \neq i}^{N_{tr}}$  via Eq.4 ▷ Calculate Task Relation
7:     Update the task-specific model  $f_\theta^i$  using the support set  $\mathcal{D}_i^s$  of task  $\tau_i$  via Eq.7 ▷ Inner-Loop Update
8:   end for
9:   Calculate relation-aware consistency score  $\mathcal{L}_{TR}(\hat{\mathcal{D}}_i^q, f_\theta^i)$  for each task ▷ Calibrate Optimization Process
10:  Update meta-learning model  $f_\theta$  using all the query sets  $\mathcal{D}^q$  in a single batch with  $\mathcal{L}_{TR}$  via Eq.8 ▷ Outer-Loop Update
11: end while
12: return solution

```

B. Proofs

In this section, we provide proofs and analyses of theorems in the main text. Before detailed proofs, we first provide the assumptions to facilitate analysis. Next, we provide proofs of Theorems 3.1, 5.1, and 5.2.

B.1. Assumptions and Discussion

We first provide the assumptions to facilitate analysis.

Assumption B.1. For each task τ_i , the representation Z_i of task τ_i is derived from the task-specific meta-data $\hat{\mathcal{D}}_i$ via the feature extractor g of meta-learning model $f_\theta = h \circ g$, where $h = (h_1, \dots, h_{N_{tr}})$. Then, we assume:

- Z_i is assumed to be uniformly distributed on $[0, 1]^k$.
- There exists a universal constant C such that for all $i, j \in N_{tr}$, we have $\|h_i - h_j\|_\infty \leq C \cdot \|Z_i - Z_j\|$.
- The relation between task τ_i and τ_j is determined by the distance between the representations Z_i and Z_j with a bandwidth σ , i.e., $m_{i,j} = \{\|Z_i - Z_j\| < \sigma\}$.
- The head \hat{h}_i from the well-learned model \mathcal{F}_θ^* such that $\mathbb{E} \left[(\hat{h}_i(g(x)) - h_i(g(x)))^2 \right] = \mathcal{O}(\frac{\mathcal{R}(\mathcal{H})}{N_i^s})$ where $\mathcal{R}(\mathcal{H})$ is the Rademacher complexity of the class \mathcal{H} .

Next, we break down and explain each part of this assumption. All the conditions within this assumption are commonly used in the machine learning community (Mohri, 2018).

The first condition is about the uniform distribution of representations, i.e., Z_i is assumed to be uniformly distributed on $[0, 1]^k$. This assumption asserts that for each task τ_i , the representation Z_i lies within the unit hypercube $[0, 1]^k$, where k is

the dimensionality of the representation. This is one of the most commonly used assumptions in machine learning (Mohri, 2018). It suggests that the representations across tasks are spread evenly in this space. The uniform distribution assumption helps simplify the analysis of how the model generalizes across tasks.

The second condition is about bounded distance between task representations, i.e., *There exists a universal constant C such that for all $i, j \in N_{tr}$, we have $\|h_i - h_j\|_\infty \leq C \cdot \|Z_i - Z_j\|$.* This assumption states that the distance between the task-specific heads h_i and h_j is bounded by a constant C times the distance between their corresponding representations Z_i and Z_j . The ∞ -norm denotes the maximum difference across each coordinate of the representations. It connects the geometry of the task representations (through Z_i and Z_j) with the behavior of the task-specific heads h_i and h_j . If the representations are close, the corresponding task heads are also close, ensuring smooth transitions and generalization between tasks.

The third condition is about task similarity, i.e., *The relation between task τ_i and τ_j is determined by the distance between the representations Z_i and Z_j with a bandwidth σ , i.e., $m_{i,j} = \{\|Z_i - Z_j\| < \sigma\}$.* It means that the relation between two tasks τ_i and τ_j is determined by the distance between their representations. Specifically, if the distance between Z_i and Z_j is smaller than a predefined threshold σ , the tasks are considered similar. The variable $m_{i,j}$ is a binary indicator that indicates whether tasks are similar. This assumption establishes a connection between the task representations and their perceived similarity, which is also a commonly used assumption.

The fourth condition is about head learning error and Rademacher complexity, i.e., *The head \hat{h}_i from the well-learned model \mathcal{F}_θ^* such that $\mathbb{E}[(\hat{h}_i(g(x)) - h_i(g(x)))^2] = \mathcal{O}(\frac{\mathcal{R}(\mathcal{H})}{N_i^{tr}})$ where $\mathcal{R}(\mathcal{H})$ is the Rademacher complexity of the class \mathcal{H} .* This assumption states that the expected squared error between the learned head \hat{h}_i and the true head h_i is bounded by a term that scales with the Rademacher complexity $\mathcal{R}(\mathcal{H})$ of the hypothesis class \mathcal{H} and inversely with the number of training examples N_i^{tr} for task τ_i . The Rademacher complexity captures the capacity of the model class to fit random noise, which is related to its ability to generalize. This assumption ties the learning error of the model to the complexity of the hypothesis class. It suggests that as the number of training examples increases, the model's learned head will get closer to the true task-specific head, and the error decreases. This is a typical assumption in generalization theory (Mohri, 2018).

B.2. Proof of Theorem 3.1

In the analyses, we consider a simple scenario involving two binary classification tasks, denoted as τ_i and τ_j . That is, we set batchsize for training as 2. The label variables for these tasks are represented by Y_i and Y_j , respectively, while X_i and X_j denote the sample variables for the two tasks. Given that these are binary classification tasks, Y_i and Y_j belong to the set of task labels $\{\pm 1\}$. It is worth noting that any multi-classification task can be decomposed into a combination of binary tasks (one against the other classes). In this proof, we focus on binary tasks to demonstrate the task confounder more simply and directly. Meanwhile, despite the two tasks are sampled from the same distribution, in this proof, we assume that these labels are drawn from two different probabilities, and the sampling probabilities of label values are balanced, i.e., $P(Y = 1) = P(Y = -1) = 0.5$. Our conclusions also hold for imbalanced distributions.

Given the set of causal factors for the entire world, a^w , the training set represents a subset of the world with causal factors $a^{tr} \subseteq A^w$. Since a^{tr} is unknown, we model a^w using a Gaussian distribution, where the probability of a causal factor indicates its likelihood of belonging to a^{tr} . For tasks τ_i and τ_j , we consider two non-overlapping sets of factors, a^i and a^j , representing knowledge in N_z dimensions. These factors are assumed to be drawn from Gaussian distributions, i.e., $a^i \sim \mathcal{N}(Y_i \cdot \mu_i, \sigma_i^2 I)$ and $a^j \sim \mathcal{N}(Y_j \cdot \mu_j, \sigma_j^2 I)$. Here, $\mu_i, \mu_j \in \mathbb{R}^{N_z}$ denote the mean vectors, while σ_i^2 and σ_j^2 denote the covariance vectors.

In this analysis, we focus on the links of different task-specific model, which reflect the performance of meta-learning model \mathcal{F}_θ and decide whether to update further. For the sake of simplicity, we define p to represent the varying correlations resulting from different task adaptations across different batches. Hence, we get:

$$\begin{aligned} P(Y_i = Y_j) &= p \\ P(Y_i \neq Y_j) &= 1 - p \end{aligned} \tag{10}$$

When p equals 0.5, it indicates that under this circumstance, the two tasks τ_i and τ_j are correlated within these environments. The objective of meta-learning adaptation is to obtain two linear models, $f_\theta^i : P(Y_i | a^i, a^j)$ and $f_\theta^j : P(Y_j | a^i, a^j)$ for τ_i and τ_j .

Next, if the task-specific model promote each other, then the optimal classifier for each task has non-zero weights for non-causal factors, i.e., the task-specific factors of another task. When training \mathcal{F}_θ using two tasks, the optimal classifier for the target task will include causal features from the other task that are non-causal factors for the target task. To demonstrate this, we assume the use of a Bayesian classifier. Using task τ_i as an example, we can derive the probability of $P(Y_i, A^i, A^j)$ with the optimal Bayesian classifier $P(Y_i|A^i, A^j)$ as follows:

$$\begin{aligned}
 P(Y_i, a^i, a^j) &= P(Y_i, a^i) \cdot P(a^j|Y_i, a^i) \\
 &= P(Y_i, a^i) \cdot P(a^j|Y_i) \\
 &= P(Y_i, a^i) \cdot \sum_{Y_j \in \{-1, 1\}} P(a^j, Y_j|Y_i) \\
 &= P(Y_i)P(a^i|Y_i) \cdot \sum_{Y_j \in \{-1, 1\}} P(a^j|Y_j)P(Y_j|Y_i)
 \end{aligned} \tag{11}$$

where the optimal Bayesian classifier $P(Y_i|A^i, A^j)$ is:

$$P(Y_i|a^i, a^j) = \frac{P(Y_i, a^i, a^j)}{P(a^i, a^j)} = \frac{P(Y_i, a^i, a^j)}{\sum_{Y_i \in \{-1, 1\}} P(Y_i, a^i, a^j)} \tag{12}$$

Assuming both a^i and a^j are drawn from Gaussian distributions, we have $P(Y_{i/j}, a^i, a^j) = \text{sigmoid} \left(\frac{\mu_i}{\sigma_i^2} a^i + \frac{\mu_j}{\sigma_j^2} a^j \right)$, where $\frac{\mu_i}{\sigma_i^2}$ and $\frac{\mu_j}{\sigma_j^2}$ are the regression vectors for the optimal Bayesian classifier.

Then, instead of assuming a direct inclusion of both factors, we assume that the weights for a^j are modulated by the similarity $\text{sim}(X_i, X_j)$. To model this, we introduce a scaling factor based on the similarity between the tasks:

$$\zeta = \text{sim}(X_i, X_j) \cdot \left(\frac{\mu_i}{\sigma_i^2} \cdot a^i + \frac{\mu_j}{\sigma_j^2} \cdot a^j \right)$$

This scaling adjusts the impact of the task-specific factors from τ_j on the classification of τ_i . As a result, the classifier's decision-making process for Y_i depends on both the task-specific factors from τ_i and τ_j , weighted by their similarity. When the tasks are highly similar ($\text{sim}(X_i, X_j)$ is large), the influence of a^j increases, leading to a stronger coupling between the tasks.

Combined with the assumptions that both a^i and a^j are drawn from Gaussian distributions, let $\zeta^+ = \frac{\mu_i}{\sigma_i^2} A^i + \frac{\mu_j}{\sigma_j^2} A^j$ and $\zeta^- = \frac{\mu_i}{\sigma_i^2} A^i - \frac{\mu_j}{\sigma_j^2} A^j$. Thus, we first obtain:

$$\begin{aligned}
 P(Y_i, a^i, a^j) &= P(Y_i, a^i) \cdot P(a^j|Y_i, a^i) \\
 &= P(Y_i)P(a^i|Y_i) \cdot \sum_{Y_j \in \{-1, 1\}} P(a^j|Y_j)P(Y_j|Y_i) \\
 &\propto e^{Y_i \cdot \frac{\mu_i}{\sigma_i^2} a^i} (p e^{Y_i \cdot \frac{\mu_j}{\sigma_j^2} a^j} + (1-p) e^{-Y_i \cdot \frac{\mu_j}{\sigma_j^2} a^j}) \\
 &= p e^{Y_i \cdot \left(\frac{\mu_i}{\sigma_i^2} a^i + \frac{\mu_j}{\sigma_j^2} a^j \right)} + (1-p) e^{Y_i \cdot \left(\frac{\mu_i}{\sigma_i^2} a^i - \frac{\mu_j}{\sigma_j^2} a^j \right)}
 \end{aligned} \tag{13}$$

Then the Bayesian classifier $P(Y_i|A^i, A^j)$ becomes:

$$P(Y_i|a^i, a^j) = \frac{1}{1 + \frac{p e^{Y_i \cdot \zeta^+} + (1-p) e^{Y_i \cdot \zeta^-}}{p e^{-Y_i \cdot \zeta^+} + (1-p) e^{-Y_i \cdot \zeta^-}}} \tag{14}$$

Next, when $p = 0.5$, i.e., the correlation between Y_i and Y_j is equal to 0.5, we get:

$$P(Y_i|a^i, a^j) = \frac{1}{1 + e^{Y_i \cdot (\zeta^+ + \zeta^-)}} = \frac{1}{1 + e^{2Y_i \cdot \left(\frac{\mu_i}{\sigma_i^2} a^i \right)}} \tag{15}$$

When $p \neq 0.5$, i.e., the correlation between Y_i and Y_j is not equal to 0.5, we get:

$$P(Y_i|a^i, a^j) = \frac{1}{1 + e^{2Y_i \cdot \zeta^+}} = \frac{1}{1 + e^{2Y_i \cdot \zeta^+}} \tag{16}$$

In both conditions, the optimal classifier for τ_i has non-zero weights for task-specific factors of τ_j with importance ζ : (i) In Eq.15, the optimal classifier for task τ_i only utilizes its factor A^i and assigns zero weights to the non-causal factor a^j which belongs to task τ_j ; (ii) In Eq.16, the optimal classifier is both for the two factors a^i and a^j . Thus, Theorem 3.1 is certified.

B.3. Proof of Theorem 5.1

To establish the proof of Theorem 5.1, we initially define a function that serves as an intermediary, which can be expressed as:

$$h_p^{in} = \frac{\sum_{i=1}^{N_{tr}} m_{ip} h_i}{\sum_{j=1}^{N_{tr}} m_{jp}}. \quad (17)$$

We proceed to delineate an event, denoted as $e_{N_{sh}}$, which is characterized by the condition $\sum_{i=1}^{N_{tr}} m_{ip} > 0$. Given our presupposition that:

$$\mathbb{E}[(\mathcal{F}_\theta^*(x) - \mathcal{F}_\theta(x))^2] = \mathbb{E}[(h_i^*(g(x)) - h_i(g(x)))^2] = \mathcal{O}\left(\frac{\mathcal{R}(\mathcal{H})}{N_i^{tr}}\right), \quad (18)$$

where g denotes the feature extractor and h denotes the classifier head for meta-learning. Here, also given the relationship $N_i^{tr} \gtrsim N_{sh}$ for every task τ_i , it follows that during the occurrence of $e_{N_{sh}}$, the following inequality holds:

$$\begin{aligned} \mathbb{E}[(h_p^{in}(g(x)) - h_p^*(g(x)))^2] &\leq \frac{\sum_{i=1}^{N_{tr}} m_{ip} \cdot \mathbb{E}[(h_i^*(g(x)) - h_i(g(x)))^2]}{(\sum_{j=1}^{N_{tr}} m_{jp})^2} \\ &\leq \frac{\max_i \mathbb{E}[(h_i^*(g(x)) - h_i(g(x)))^2]}{\sum_{j=1}^{N_{tr}} m_{jp}} \\ &= \mathcal{O}\left(\frac{\mathcal{R}(\mathcal{H})}{N_{sh} \sum_{j=1}^{N_{tr}} m_{jp}}\right). \end{aligned} \quad (19)$$

Furthermore, given that $\|h_i - h_j\|_\infty \leq C \cdot \|Z_i - Z_j\| \leq C \cdot \sigma$ when $\|Z_i - Z_j\| \leq \sigma$, we can assert that within the scenario $e_{N_{sh}}$, the inequality $|h_k^{in} - h_k| \leq C \cdot \sigma$ is valid. Conversely, for the complementary event $e_{N_{sh}}^c$, the denominator is nullified by definition, rendering $h_k^{in}(g(x)) = 0$ and thus:

$$|h_p^{in}(g(x)) - h_p(g(x))|^2 = (h_p)^2(g(x)) \leq (C \cdot \sigma)^2 + (h_p)^2(g(x)) \cdot \mathbf{1}_{e_{N_{sh}}^c}. \quad (20)$$

As a result, we derive that:

$$\mathbb{E}[(h_p^* - h_p)^2] \lesssim \mathbb{E}\left[\frac{\mathcal{R}(\mathcal{H})}{N_{sh} \sum_{j=1}^{N_{tr}} m_{jp}} \cdot \mathbf{1}_{e_{N_{sh}}}\right] + \sigma^2 + \mathbb{E}\left[(h_p)^2(g(x)) \cdot \mathbf{1}_{e_{N_{sh}}^c}\right]. \quad (21)$$

For the initial term, let $S = \sum_{i=1}^{N_{tr}} \mathbf{1}\{\|Z_k - Z_i\| < \sigma\}$. Considering Z^{un} are uniformly distributed over $[0, 1]^p$, S follows a binomial distribution $\mathcal{B}(N_{tr}, \varepsilon)$, where $\varepsilon = \mathbb{P}(\|Z - Z_k\| < \sigma)$. Utilizing the properties of the binomial distribution, we establish that:

$$\mathbb{E}\left[\frac{\mathbf{1}\{S > 0\}}{S}\right] \lesssim \frac{1}{N_{tr}\varepsilon} \lesssim \frac{1}{N_{tr}\sigma^k}. \quad (22)$$

Hence, the initial term is bounded by:

$$\mathbb{E}\left[\frac{\mathcal{R}(\mathcal{H})}{N_{sh} \sum_{j=1}^{N_{tr}} m_{jp}} \cdot \mathbf{1}_{e_{N_{sh}}}\right] \lesssim \frac{\mathcal{R}(\mathcal{H})}{N_{sh} N_{tr} \sigma^k}, \quad (23)$$

The third term can be bounded in a similar fashion:

$$\begin{aligned} &\mathbb{E}\left[(h_p)^2(g(x)) \cdot \mathbf{1}_{e_{N_{sh}}^c}\right] \\ &\leq \sup(h_p)^2(g(x)) \mathbb{E}[(1 - q)^{N_{tr}}] \\ &\lesssim \sup(h_p)^2(g(x)) \frac{1}{N_{tr}q} \\ &\lesssim \frac{1}{N_{tr}\sigma^k}. \end{aligned} \quad (24)$$

By amalgamating all components, we arrive at:

$$\mathbb{E}[(h_p^* - h_p)^2] \lesssim \sigma^2 + \frac{\mathcal{R}(\mathcal{H})/N_{sh}}{N_{tr}\sigma^k}. \quad (25)$$

Given that ℓ is Lipschitz continuous with respect to its first parameter, the following inequality is obtained:

$$\begin{aligned} & \mathbb{E}_{(x,y) \sim P_t} [\ell(\hat{f}_\theta^{(t)}(x), y)] - \mathbb{E}_{(x,y) \sim P_t} [\ell(f_\theta^{(t)}(x), y)] \\ & \leq \mathbb{E} [|\hat{h}^{(t)} - h^{(t)}|] \\ & \leq \sqrt{\mathbb{E}[(\hat{h}^{(t)} - h^{(t)})^2]} \\ & \lesssim \sigma + \sqrt{\frac{\mathcal{R}(\mathcal{H})/N_{sh}}{N_{tr}\sigma^k}}. \end{aligned} \quad (26)$$

So far, we have completed the proof of Theorem 5.1.

B.4. Proof of Theorem 5.2

If we treat all training tasks as equally important, meaning $m_{ip} = 1$ for all τ_i and τ_p , we can express the estimator h_p as:

$$h_p = \frac{\sum_{i=1}^{N_{tr}} m_{ip} h_p}{\sum_{j=1}^{N_{tr}} m_{jp}} = \frac{1}{N_{tr}} \sum_{i=1}^{N_{tr}} h_p. \quad (27)$$

To show that this estimator performs worse than the optimal estimator h_p^* in the minimax sense which is the classifier head of the trained model \mathcal{F}_θ^* , we need to find an $h \in \mathcal{H}$ such that $\mathcal{R}_h(h^{sum}(f(x))) = \Omega(1)$ even as $N_i^{tr}, N_{tr} \rightarrow \infty$. Here, we denote h^{sum} as the average estimator of all tasks.

Consider the following setting: let $d \sim \mathcal{U}(0, 1)$ be uniformly distributed on $(0, 1)$ and let $g(x) \sim \mathcal{N}(0, 1)$ be normally distributed with mean 0 and variance 1. Define $h^d(g(x)) = d \cdot g(x)$. Under this setting, the average estimator h^{sum} becomes $h^{sum} = \frac{1}{2}g(x)$ since the expectation of d over a uniform distribution on $[0, 1]$ is $\frac{1}{2}$. To compute the risk, we calculate:

$$\mathbb{E}[(h^{sum}(g(x)) - h^d(g(x)))^2] = \mathbb{E}[(\frac{1}{2}g(x) - d \cdot g(x))^2]. \quad (28)$$

Simplifying inside the expectation, we get:

$$\mathbb{E} \left[\left(\frac{1}{2} - d \right) g(x) \right]^2 = \mathbb{E}[(\frac{1}{2} - d)^2] \cdot \mathbb{E}[g(x)^2]. \quad (29)$$

Since $\mathbb{E}[g(x)^2] = 1$ (the variance of $g(x)$), we need to find $\mathbb{E}[(\frac{1}{2} - d)^2]$:

$$\mathbb{E} \left[\left(\frac{1}{2} - d \right)^2 \right] = \int_0^1 \left(\frac{1}{2} - d \right)^2 dd. \quad (30)$$

Evaluating this integral, we have:

$$\begin{aligned} & \mathbb{E} \left[\left(\frac{1}{2} - d \right)^2 \right] \\ & = \int_0^1 (\frac{1}{4} - d + d^2) dd \\ & = \left[\frac{1}{4}d - \frac{d^2}{2} + \frac{d^3}{3} \right]_0^1 \\ & = \frac{1}{4} - \frac{1}{2} \cdot \frac{1}{2} + \frac{1}{3} = \frac{1}{12}. \end{aligned} \quad (31)$$

Therefore, we get:

$$\mathbb{E}[(h^{sum}(g(x)) - h^d(g(x)))^2] = \frac{1}{12} = \Omega(1). \quad (32)$$

Since the model $\mathcal{F}_\theta = h \circ g$ and the excess risk with task relation matrix \mathcal{M} is denoted by $r(\mathcal{F}_\theta^*, \mathcal{M}) = \sum_{(x,y) \in \mathcal{D}^{te}} [\ell(\mathcal{F}_\theta^*(x), y; \mathcal{M}) - \ell(\mathcal{F}_\theta(x), y; \mathcal{M})]$, we have:

$$\inf_{\mathcal{F}_\theta^*} \sup_{h \in \mathcal{H}} r(\mathcal{F}_\theta^*, \mathcal{M}) - \inf_{\mathcal{F}_\theta^*} \sup_{h \in \mathcal{H}} r(\mathcal{F}_\theta^*, \check{\mathcal{M}}) < 0. \quad (33)$$

This completes the proof.

C. Practical Implementation of Meta-Learning

For optimization, the standard interpretation, i.e., understanding meta-learning from “learning a good model initialization”, treats meta-learning as a second-order derivative process, while in practice, single-level updates are commonly used. Specifically, meta-learning models are typically updated via implicit gradients (Rajeswaran et al., 2019; Barrett & Dherin, 2020; Khadka et al., 2022; Flennergaard et al., 2019; Lee et al., 2021), differentiable proxies (Choe et al., 2024; Bohdal et al., 2021; Boutilier et al., 2020; Liu et al., 2022), or single-layer approximations (Nichol & Schulman, 2018; Rajendran et al., 2020; Nichol et al., 2018) (Appendix C), which aggregate multi-tasks gradients into a single optimization step.

For a simple but clear explanation, we set the parameters of the inner loop as ϕ and the parameters of the outer loop as θ according to the concept of “learning to learn”. Then, the inner optimization problem is assumed to be $\phi^*(\theta) = \arg \min_{\phi} \mathcal{L}_{\text{inner}}(\theta, \phi)$, where θ is the outer parameter, ϕ is the parameter of inner loop, and $\mathcal{L}_{\text{inner}}$ is the loss function.

Implicit Gradient The implicit gradient method calculates the outer gradient $\nabla_{\theta} \mathcal{L}_{\text{outer}}(\theta, \phi^*(\theta))$ by solving the following equation:

$$\nabla_{\theta} \phi^*(\theta) = - [\nabla_{\phi}^2 \mathcal{L}_{\text{inner}}(\theta, \phi^*(\theta))]^{-1} \nabla_{\theta \phi}^2 \mathcal{L}_{\text{inner}}(\theta, \phi^*(\theta)), \quad (34)$$

where $\nabla_{\phi}^2 \mathcal{L}_{\text{inner}}$ is the Hessian matrix with respect to ϕ for the inner loss function. Then, the outer gradient is computed using the chain rule:

$$\nabla_{\theta} \mathcal{L}_{\text{outer}}(\theta, \phi^*(\theta)) = \nabla_{\phi} \mathcal{L}_{\text{outer}}(\theta, \phi^*(\theta)) \cdot \nabla_{\theta} \phi^*(\theta) + \nabla_{\theta} \mathcal{L}_{\text{outer}}(\theta, \phi^*(\theta)) \quad (35)$$

This allows the outer parameter θ to be updated without explicitly solving the inner loop optimization.

Differentiable Proxies In some applications, the inner optimization objective $\mathcal{L}_{\text{inner}}(\theta, \phi)$ may be difficult to compute or non-differentiable. To simplify this, a differentiable proxy function $\tilde{\mathcal{L}}_{\text{inner}}(\theta, \phi)$ can be used as a substitute:

$$\tilde{\mathcal{L}}_{\text{inner}}(\theta, \phi) \approx \mathcal{L}_{\text{inner}}(\theta, \phi). \quad (36)$$

Then, the proxy function is used for inner loop optimization:

$$\phi^*(\theta) = \arg \min_{\phi} \tilde{\mathcal{L}}_{\text{inner}}(\theta, \phi). \quad (37)$$

The outer loop optimization still targets $\mathcal{L}_{\text{outer}}(\theta, \phi^*(\theta))$.

Single-level Approximation The bi-level optimization problem is simplified. The inner loop optimization becomes:

$$\phi^i = \phi - \alpha \nabla_{\phi} \mathcal{L}_{\text{inner}}(\theta, \phi), \quad (38)$$

and the outer loop optimization is:

$$\min_{\theta} \sum_{i=1}^N \mathcal{L}_{\text{outer}}(\theta, \phi^i). \quad (39)$$

In the single-level approximation, the update from the inner loop optimization is treated as a fixed value, and ϕ is no longer iteratively optimized. The outer loop directly uses the updated ϕ^i with:

$$\min_{\theta} \sum_{i=1}^N \mathcal{L}_{\text{outer}}(\theta, \phi - \alpha \nabla_{\phi} \mathcal{L}_{\text{inner}}(\theta, \phi)). \quad (40)$$

In the optimization process of meta-learning model \mathcal{F}_θ , the gradient information on all tasks is integrated into a single optimization step and directly used to update the global parameter θ , which means that the model \mathcal{F}_θ is not gradually learned and optimized through internal and external loops, but directly adapted to multiple tasks through a single process. Therefore, the actual meta-learning model update method is more like a single-layer optimization process rather than true “learning to learn”, i.e., it does not strictly follow the theoretical two-layer optimization framework.

D. More Discussion

D.1. Universality and Effectiveness of Task Relations

TRLearner uses task relations and relation-aware consistency regularization to refine the meta-learning optimization. It assumes that similar tasks often share similar predictive functions, and thus enforces the outputs of task-specific models for similar tasks to be similar. Notably, although TRLearner computes task similarity to build a task relationship matrix, it does not require all tasks in a batch to be similar. Instead, TRLearner’s strength lies in leveraging inter-task relationships to highlight useful information—effectively filtering task information—and can work with any combination of tasks. Here, we discuss performance under both diverse and homogeneous task conditions from two angles: task construction in meta-learning and the sources of TRLearner’s effectiveness.

According to Section 2, we assume all tasks—including the meta-training dataset \mathcal{D}_{tr} and the meta-test dataset \mathcal{D}_{te} —are drawn from the same fixed distribution $p(\mathcal{T})$, with no class overlap between \mathcal{D}_{tr} and \mathcal{D}_{te} . According to Baxter’s multi-task learning theorem (Baxter, 1997), when a set of tasks sampled i.i.d. from the same distribution share certain structural commonalities (e.g., a common hypothesis space or representation structure), learning these tasks jointly can yield a lower-complexity representation space (Standley et al., 2020). This implies that the construction of meta-tasks itself provides theoretical support for TRLearner’s learning. Furthermore, based on analyses by Maurer and Pentina (Maurer et al., 2016), if the meta-learner encounters multiple tasks from the same distribution during meta-training and obtains a “low-complexity” unified representation, then subsequent tasks drawn from the same distribution can achieve better generalization with fewer samples. In addition, we build an adaptive sampler following (Wang et al., 2024a) to obtain meta-data and extract task relationships. By selecting tasks under constraints of within-class compactness and between-class separability, the sampler makes it more challenging to extract structural commonalities among tasks. Under these conditions, leveraging task relations enables the model to better capture the underlying structural commonalities of the tasks. Thus, regardless of the initial task distribution, TRLearner can well calibrate the meta-learning optimization process and guide it to obtain effective representations.

Secondly, TRLearner’s effectiveness lies in its ability to filter and emphasize task information through inter-task relationships, rather than directly learning task-to-task similarities. Under limited data conditions, TRLearner leverages task relationships derived from meta-data to provide the model with additional insights, preventing it from over-focusing on task-specific features and thus maintaining a balance with over-parameterized networks. When data is abundant or tasks are diverse, these relationships guide the model to focus on shared, effective information across tasks. Grounded in causal invariance theory (Pearl, 2009), such shared information also proves beneficial for downstream tasks. Consequently, even when tasks are largely unrelated, TRLearner can increase the weight of inter-task relationships to suppress task-specific factors (e.g., environmental features) and highlight shared factors (e.g., entity-related features) that enhance generalization to downstream tasks. Moreover, both theoretical and empirical evidence from Section 5 and Section 6 demonstrate that TRLearner remains effective across various benchmark datasets and task distributions without relying on prior assumptions about the task distribution.

D.2. How Task Relation Works From Task Information

In meta-learning, the balance between task generality and task complementarity is crucial. Task generality refers to the task-shared knowledge between different tasks, which allows the model to learn general features and generalize to unseen tasks. For example, different classes may share similar visual features, e.g., edges, textures, or shapes. By identifying these task-shared features, the model can adapt to unseen tasks more quickly (Wilder et al., 2020). In contrast, task complementarity refers to the relationship between different tasks, whereby learning this, the model can acquire more discriminative knowledge. This complementarity can help the model identify and utilize effective features to improve performance on specific tasks (Zheng et al., 2021). For example, in multi-task learning, a model may learn classification and detection tasks at the same time. The classification task may help the model learn the general features of the object, while the detection task may emphasize the location and size of the object. This complementary knowledge learned by the model can improve the overall performance of the model on both tasks.

Therefore, on the one hand, the model needs to be able to identify and utilize common knowledge across tasks to adapt to new tasks quickly; on the other hand, the model also needs to be able to learn task-specific knowledge to improve performance and accuracy on specific tasks. However, most existing methods focus on task generality and ignore task complementarity, which may cause the model to ignore important discriminative features and damage model performance. In this study, one reason for how introducing task relations works is to use the power of task relations to force the model to

learn task complementarity, which has been ignored in the past. Task relations cover the similarities or correlations between different tasks. To illustrate this concept, we take the drug response prediction task as an example: identifying each cell line is considered a separate task. If these cell lines show similar gene expression profiles or belong to the same cancer type, they are considered to be related, that is, there exist task relations.

E. Datasets

In this section, we elucidate the datasets encompassed within the four experimental scenarios.

E.1. Regression

We select the Regression problem with two datasets as our inaugural experimental scenario, i.e., Sinusoid and Harmonic datasets. The datasets here consist of data points generated by a variety of sinusoidal functions, with a minimal number of data points per class or pattern. Each data point comprises an input value x and its corresponding target output value y . Typically, the input values for these data points fluctuate within a confined range, such as between 0 and 2π .

In our experiment, we enhance the complexity of the originally straightforward problem by incorporating noise. Specifically, for Sinusoid regression, we adhere to the configuration proposed by (Jiang et al., 2022; Wang et al., 2023), where the data for each task is formulated as $A \sin(\omega \cdot x) + b + \epsilon$, with A ranging from 0.1 to 5.0, ω from 0.5 to 2.0, and b from 0 to 2π . Subsequently, we introduce Gaussian observational noise with a mean of 0 and a variance of 0.3 for each data point derived from the target task. Similarly, the Harmonic dataset (Lacoste et al., 2018) is a synthetic dataset sampled from the sum of two sine waves with different phases, amplitudes, and a frequency ratio of 2: $f(x) = a_1 \sin(\omega x + b_1) + a_2 \sin(2\omega x + b_2)$, where $y \sim \mathcal{N}(f(x), \sigma_y^2)$. Each task in the Harmonic dataset is sampled with $\omega \sim \mathcal{U}(5, 7)$, $(b_1, b_2) \sim \mathcal{U}(0, 2\pi)^2$, and $(a_1, a_2) \sim \mathcal{N}(0, 1)^2$. This process finalizes the construction of the dataset for this scenario.

E.2. Image Classification

For our second scenario, image classification, we select four benchmark datasets with two experimental settings, including standard few-shot learning (SFSL) with miniImagenet (Vinyals et al., 2016; Lin et al., 2023; Zhang et al., 2024) and Omniglot (Lake et al., 2019), and cross-domain few-shot learning (CFSL) with CUB (Welinder et al., 2010) and Places (Zhou et al., 2017). We now provide an overview of the four datasets in this scenario.

- miniImagenet consists of 50,000 training images and 10,000 testing images, evenly spread across 100 categories. The first 80 of these categories are designated for training, while the final 20 are reserved for testing, with the latter never encountered during the training phase. All images are sourced from Imagenet.
- Omniglot is designed to foster the development of learning algorithms that mimic human learning processes. It encompasses 1,623 unique handwritten characters from 50 distinct alphabets, each drawn by 20 different individuals through Amazon’s Mechanical Turk. Each character image is paired with stroke data sequences $[x, y, t]$ and temporal coordinates (t) in milliseconds.
- CUB is extensively utilized for tasks involving the fine-grained differentiation of visual categories. It encompasses a collection of 11,788 photographs, categorized into 200 distinct bird species, with 5,994 images designated for training purposes and 5,794 for testing. The dataset provides comprehensive annotations for each photograph, including a single subcategory label, the precise locations of 15 parts, 312 binary attributes, and a single bounding box. We split all the data into 100/50/50 classes for meta-training/validation/testing.
- Places is a comprehensive image collection designed for the task of scene recognition, a critical area within the field of computer vision. It boasts an extensive library of over 2.5 million images, meticulously categorized into 205 unique scene categories. Each image is meticulously curated to represent a wide array of natural and man-made environments, providing a rich tapestry of visual data for training and evaluating machine learning models. We split them into 103/51/51 classes for meta-training/validation/testing.

Note that the models in the SFSL setting are trained and tested on their evaluation datasets, while the models in the CFSL setting are trained on the miniImagenet dataset and then tested on the CUB or Places datasets.

Table 6. Full results (accuracy \pm 95% confidence interval) of image classification on (5-way 1-shot and 5-way 5-shot) miniImagenet and (20-way 1-shot and 20-way 5-shot) Omniglot. The best results are highlighted in **bold**. The “+” and “-” indicate the performance changes after adding MetaMix, Dropout-Bins, and MetaCRL. The “\” denotes that the result is not reported.

MODEL	OMNIGLOT		MINIIMAGENET		MINIIMAGENET \rightarrow CUB		MINIIMAGENET \rightarrow PLACES	
	20-WAY 1-SHOT	20-WAY 5-SHOT	5-WAY 1-SHOT	5-WAY 5-SHOT	5-WAY 1-SHOT	5-WAY 5-SHOT	5-WAY 1-SHOT	5-WAY 5-SHOT
META-TRANS	87.39 \pm 0.51	92.13 \pm 0.19	35.19 \pm 1.58	54.31 \pm 0.88	36.21 \pm 1.36	52.78 \pm 1.91	31.97 \pm 0.52	\
MR-MAML	89.28 \pm 0.59	95.01 \pm 0.23	35.01 \pm 1.60	55.06 \pm 0.91	35.76 \pm 1.27	50.85 \pm 1.65	31.23 \pm 0.48	46.41 \pm 1.22
iMOL	92.89 \pm 0.44	97.58 \pm 0.34	36.27 \pm 1.54	57.14 \pm 0.87	37.14 \pm 1.17	51.21 \pm 1.01	32.44 \pm 0.65	47.55 \pm 0.94
OOD-MAML	93.01 \pm 0.50	98.06 \pm 0.27	37.43 \pm 1.47	57.68 \pm 0.85	39.62 \pm 1.34	52.65 \pm 0.77	35.52 \pm 0.69	\
ROTOGBML	92.77 \pm 0.69	98.42 \pm 0.31	39.32 \pm 1.62	58.42 \pm 0.83	41.27 \pm 1.24	\	31.23 \pm 0.48	\
MAML	87.15 \pm 0.61	93.51 \pm 0.25	33.16 \pm 1.70	51.95 \pm 0.97	33.62 \pm 1.18	49.15 \pm 1.32	29.84 \pm 0.56	43.56 \pm 0.88
MAML + META-AUG	89.77 \pm 0.62	94.56 \pm 0.20	34.76 \pm 1.52	54.12 \pm 0.94	34.58 \pm 1.24	\	30.57 \pm 0.63	\
MAML + METAMIX	91.97 \pm 0.51	97.95 \pm 0.17	38.97 \pm 1.81	58.96 \pm 0.95	36.29 \pm 1.37	\	31.76 \pm 0.49	\
MAML + DROPOUT-BINS	92.89 \pm 0.46	98.03 \pm 0.15	39.66 \pm 1.74	59.32 \pm 0.93	37.41 \pm 1.12	\	33.69 \pm 0.78	\
MAML + METACRL	93.00 \pm 0.42	98.39 \pm 0.18	41.55 \pm 1.76	60.01 \pm 0.95	38.16 \pm 1.27	\	35.41 \pm 0.53	\
MAML + TRLEARNER	94.23 \pm 0.56	98.74 \pm 0.24	42.86 \pm 1.83	61.74 \pm 0.96	40.54 \pm 1.26	54.51 \pm 0.66	36.12 \pm 0.64	48.22 \pm 0.95
PROTONET	89.15 \pm 0.46	94.01 \pm 0.19	33.76 \pm 0.95	50.28 \pm 1.31	34.28 \pm 1.14	48.62 \pm 0.99	30.43 \pm 0.57	43.40 \pm 0.88
PROTONET + META-AUG	90.87 \pm 0.52	94.17 \pm 0.25	33.95 \pm 0.98	50.85 \pm 1.16	35.67 \pm 1.31	\	31.27 \pm 0.62	\
PROTONET + METAMIX	91.08 \pm 0.51	94.32 \pm 0.29	34.23 \pm 1.55	51.77 \pm 0.89	37.19 \pm 1.24	\	31.85 \pm 0.64	\
PROTONET + DROPOUT-BINS	92.13 \pm 0.48	94.89 \pm 0.23	34.62 \pm 1.54	52.13 \pm 0.97	37.86 \pm 1.36	\	32.59 \pm 0.53	\
PROTONET + METACRL	93.09 \pm 0.25	95.34 \pm 0.18	34.97 \pm 1.60	53.09 \pm 0.93	38.67 \pm 1.25	\	33.82 \pm 0.71	\
PROTONET + TRLEARNER	94.56 \pm 0.39	96.76 \pm 0.24	35.45 \pm 1.72	54.62 \pm 0.95	39.41 \pm 1.26	55.13 \pm 1.32	34.54 \pm 0.64	49.00 \pm 0.74
ANIL	89.17 \pm 0.56	95.85 \pm 0.19	34.96 \pm 1.71	52.59 \pm 0.96	35.74 \pm 1.16	49.96 \pm 1.55	31.64 \pm 0.57	44.90 \pm 1.32
ANIL + META-AUG	90.46 \pm 0.47	96.31 \pm 0.17	35.44 \pm 1.73	56.46 \pm 0.95	36.32 \pm 1.28	\	32.58 \pm 0.64	\
ANIL + METAMIX	92.88 \pm 0.51	98.36 \pm 0.13	37.82 \pm 1.75	59.03 \pm 0.93	36.89 \pm 1.34	\	33.72 \pm 0.61	\
ANIL + DROPOUT-BINS	92.82 \pm 0.49	98.42 \pm 0.14	38.09 \pm 1.76	59.17 \pm 0.94	38.24 \pm 1.17	\	33.94 \pm 0.66	\
ANIL + METACRL	92.91 \pm 0.52	98.77 \pm 0.15	38.55 \pm 1.81	59.68 \pm 0.94	39.68 \pm 1.32	\	34.47 \pm 0.52	\
ANIL + TRLEARNER	93.24 \pm 0.48	99.28 \pm 0.21	38.73 \pm 1.84	60.42 \pm 0.95	41.96 \pm 1.24	56.22 \pm 1.25	35.68 \pm 0.61	47.30 \pm 1.30
METASGD	87.81 \pm 0.61	95.52 \pm 0.18	33.97 \pm 1.34	52.14 \pm 0.92	33.65 \pm 1.13	50.00 \pm 0.84	29.83 \pm 0.66	45.21 \pm 0.79
METASGD + META-AUG	88.56 \pm 0.57	96.73 \pm 0.14	35.76 \pm 0.91	58.65 \pm 0.94	34.73 \pm 1.32	\	31.49 \pm 0.54	\
METASGD + METAMIX	93.44 \pm 0.45	98.24 \pm 0.16	40.28 \pm 1.64	60.19 \pm 0.96	35.26 \pm 1.21	\	32.76 \pm 0.59	\
METASGD + DROPOUT-BINS	93.93 \pm 0.40	98.49 \pm 0.12	40.31 \pm 0.96	60.73 \pm 0.92	37.49 \pm 1.37	\	33.21 \pm 0.67	\
METASGD + METACRL	94.12 \pm 0.43	98.60 \pm 0.15	41.22 \pm 1.41	60.88 \pm 0.91	38.61 \pm 1.25	\	35.83 \pm 0.63	\
METASGD + TRLEARNER	94.57 \pm 0.49	99.43 \pm 0.22	41.64 \pm 0.94	62.43 \pm 0.96	39.58 \pm 1.13	57.56 \pm 1.12	36.42 \pm 0.54	48.20 \pm 0.69
T-NET	87.66 \pm 0.59	95.67 \pm 0.20	33.69 \pm 1.72	54.04 \pm 0.99	34.82 \pm 1.17	\	28.77 \pm 0.48	\
T-NET + METAMIX	93.16 \pm 0.48	98.09 \pm 0.15	39.18 \pm 1.73	59.13 \pm 0.99	35.42 \pm 1.28	\	30.54 \pm 0.57	\
T-NET + DROPOUT-BINS	93.54 \pm 0.49	98.27 \pm 0.14	39.06 \pm 1.72	59.25 \pm 0.97	37.22 \pm 1.37	\	31.28 \pm 0.61	\
T-NET + METACRL	93.81 \pm 0.52	98.56 \pm 0.14	40.08 \pm 1.74	59.40 \pm 0.98	37.49 \pm 1.14	\	32.37 \pm 0.55	\
T-NET + TRLEARNER	94.33 \pm 0.54	98.84 \pm 0.17	40.31 \pm 1.75	61.26 \pm 0.97	40.64 \pm 1.29	\	34.76 \pm 0.62	\

E.3. Drug Activity Prediction

In our third scenario, concerning drug activity prediction, we align with the data partitioning delineated in (Martin et al., 2019; Jiang et al., 2022). We extract 4276 tasks from the ChEMBL database (Gaulton et al., 2012) to constitute our baseline dataset, which is preprocessed in accordance with the guidelines set forth by (Martin et al., 2019).

ChEMBL is a comprehensive database utilized extensively in chemical biology and drug research, housing a wealth of biological activity and chemical information. It contains over 1.9 million compounds, more than 2 million bioactivity assay results, and thousands of biological targets, all meticulously structured. This includes the structural data of drug compounds, bioactivity assay outcomes, and descriptions of drug targets. Following the approach in (Martin et al., 2019), we segregate the training compounds in the support set from the testing compounds in the query set, with the meta-training, meta-validation, and meta-testing task distribution being 4100, 76, and 100, respectively.

E.4. Pose Prediction

For our final scenario, we select the Pascal 3D dataset (Xiang et al., 2014) as our benchmark and process it accordingly. We randomly select 50 objects for meta-training and an additional 15 objects for meta-testing.

The Pascal 3D dataset is composed of outdoor images, featuring 12 classes of rigid objects chosen from the PASCAL VOC 2012 dataset, each annotated with pose information such as azimuth, elevation, and distance to the camera. The dataset also includes pose-annotated images for these 12 categories from the ImageNet dataset. For the pose prediction task, we preprocess it to include 50 categories for meta-training and 15 for meta-testing, with each category comprising 100 grayscale images, each measuring 128 \times 128 pixels.

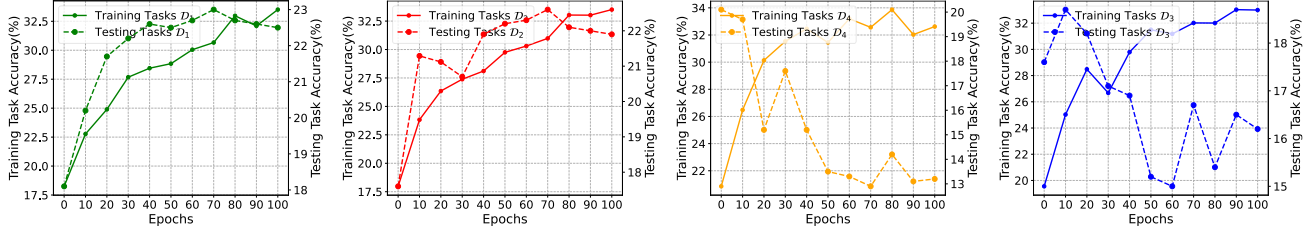


Figure 6. Motivating evidence about the performance of the model on \mathcal{D}_1 – \mathcal{D}_4 . Each group of tasks has a different sampling score, i.e., 0.79, 0.72, 0.31, and 0.29 respectively. Higher sampling scores indicate greater task complexity.

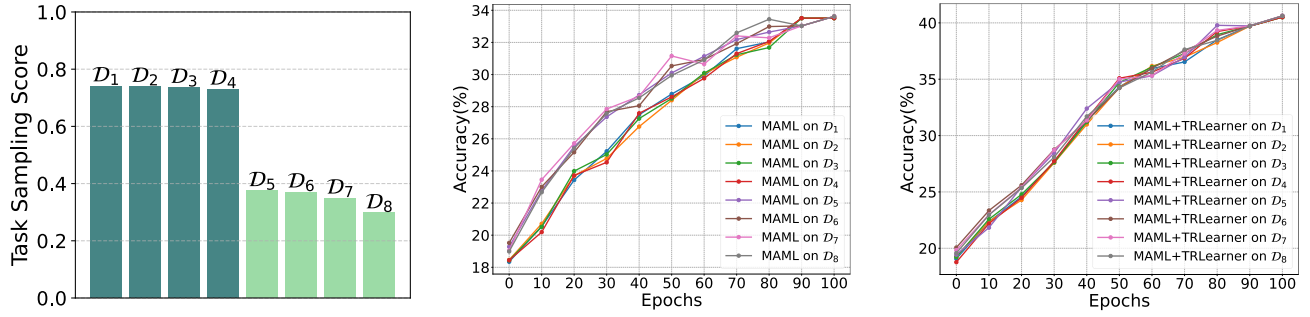


Figure 7. Performance comparison of the motivating experiment after introducing TRLearner. **Left:** The score of the sampled tasks. **Middle:** Results of motivating experiment with MAML. **Right:** Results of motivating experiment with MAML+TRLearner.

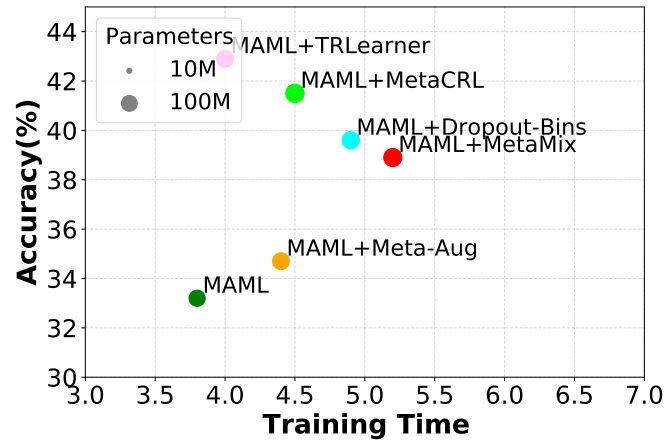


Figure 8. Trade-off performance comparison on miniImagenet. We select MAML as the meta-learning baseline.

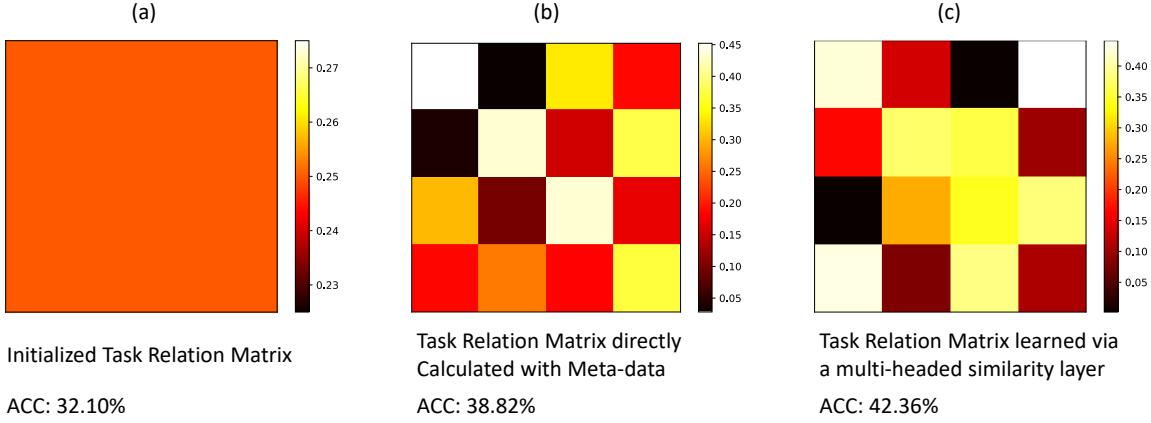


Figure 9. Task Relation Visualization. (a), (b), and (c) respectively represent the initialized task relation matrix, the task relation matrix directly calculated based on the extracted task-specific meta-data, and the task relation matrix further learned using a multi-headed similarity layer. Note that when we visualize the task relation matrix, we normalize the values in each matrix, i.e., the sum of similarity weights between the same task and other tasks is 1.

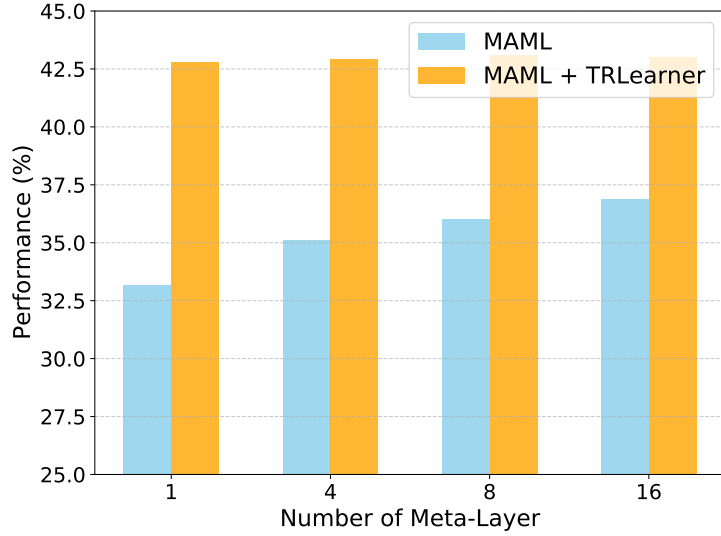


Figure 10. Performance of meta-learning model under the different number of meta-layers. The bars represent the performance of MAML with different meta-layers, i.e., 1, 4, 8, and 16.

Table 7. Full results on drug activity prediction. “Mean”, “Mde.”, and “> 0.3” are the mean, the median value of R^2 , and the number of analyzes for $R^2 > 0.3$ stands as a reliable indicator in pharmacology. The best results are highlighted in **bold**.

MODEL	GROUP 1			GROUP 2			GROUP 3			GROUP 4			GROUP 5 (AVE)		
	MEAN	MED.	> 0.3	MEAN	MED.	> 0.3									
MAML	0.371	0.315	52	0.321	0.254	43	0.318	0.239	44	0.348	0.281	47	0.341	0.260	45
MAML+DROPOUT-BINS	0.410	0.376	60	0.355	0.257	48	0.320	0.275	46	0.370	0.337	56	0.380	0.314	52
MAML+METACRL	0.413	0.378	61	0.360	0.261	50	0.334	0.282	51	0.375	0.341	59	0.371	0.316	56
MAML+TRLEARNER	0.418	0.380	62	0.366	0.263	52	0.342	0.285	52	0.379	0.339	59	0.378	0.319	56
PROTONEt	0.361	0.306	51	0.319	0.269	47	0.309	0.264	44	0.339	0.289	47	0.332	0.282	47
PROTONEt + DROPOUT-BINS	0.391	0.358	59	0.336	0.271	48	0.314	0.268	45	0.376	0.341	57	0.354	0.309	52
PROTONEt + METACRL	0.409	0.398	62	0.379	0.292	52	0.331	0.300	52	0.385	0.356	59	0.381	0.336	56
PROTONEt + TRLEARNER	0.436	0.402	63	0.384	0.306	54	0.357	0.313	53	0.398	0.372	61	0.393	0.348	57
ANIL	0.355	0.296	50	0.318	0.297	49	0.304	0.247	46	0.338	0.301	50	0.330	0.284	48
ANIL+METAMIX	0.347	0.292	49	0.302	0.258	45	0.301	0.282	47	0.348	0.303	51	0.327	0.284	48
ANIL+DROPOUT-BINS	0.394	0.321	53	0.338	0.271	48	0.312	0.284	46	0.368	0.297	50	0.350	0.271	49
ANIL+METACRL	0.401	0.339	57	0.341	0.277	49	0.312	0.291	48	0.371	0.305	53	0.356	0.303	51
ANIL+TRLEARNER	0.402	0.341	57	0.347	0.276	49	0.320	0.296	48	0.374	0.306	53	0.364	0.304	51
METASGD	0.389	0.305	50	0.324	0.239	46	0.298	0.235	41	0.353	0.317	52	0.341	0.274	47
METASGD + METAMIX	0.364	0.296	49	0.312	0.267	48	0.271	0.230	45	0.338	0.319	51	0.321	0.278	48
METASGD + DROPOUT-BINS	0.390	0.302	57	0.358	0.339	56	0.316	0.269	43	0.360	0.311	50	0.356	0.315	51
METASGD + METACRL	0.398	0.295	59	0.356	0.340	59	0.321	0.271	44	0.373	0.324	55	0.362	0.307	54
METASGD + TRLEARNER	0.403	0.314	61	0.367	0.351	60	0.345	0.284	46	0.385	0.328	56	0.374	0.319	55

F. Baselines

In this paper, we focus on the generalization of meta-learning and select four optimization-based meta-learning methods as the backbone for evaluating the performance of TRLearner, i.e., MAML (Finn et al., 2017), MetaSGD (Li et al., 2017), ANIL (Raghu et al., 2019a), and T-Net (Lee & Choi, 2018). Meanwhile, we also select multiple baselines for comparison, including regularizers which handle meta-learning generalization, i.e., Meta-Aug (Rajendran et al., 2020), MetaMix (Yao et al., 2021), Dropout-Bins (Jiang et al., 2022) and MetaCRL (Wang et al., 2023), and the SOTA methods which are newly proposed for generalization, i.e., Meta-Trans (Bengio et al., 2019), MR-MAML (Yin et al., 2020), iMOL (Wu et al., 2023), OOD-MAML (Jeong & Kim, 2020), and RotoGBML (Zhang et al., 2023). Here, we briefly introduce all the methods used in our experiments.

MAML (Model-Agnostic Meta-Learning) is a widely used meta-learning algorithm that seeks to find a model initialization capable of being fine-tuned to new tasks with a few gradient steps. It focuses on learning an initialization that facilitates rapid adaptation.

MetaSGD is a meta-learning algorithm that adapts the learning rate during the meta-training process. It focuses on optimizing the learning rate, potentially improving the model’s ability to generalize across tasks.

ANIL aims to reduce the number of inner loop iterations during meta-learning. It optimizes the meta-learner by minimizing the reliance on costly inner loop optimization steps, aiming for more efficient training.

T-Net (Task-Agnostic Network) learns a shared representation across tasks. It aims to develop a task-agnostic feature extractor that captures common patterns in different tasks, thereby improving generalization.

ProtoNet (Prototypical Networks) learns to map input data into an embedding space and represent each class by a “prototype,” which is the mean vector of its support samples in that space. During prediction, a new sample is also embedded and then classified by finding the class prototype closest to it in terms of distance.

Meta-Aug is built by using data augmentation in the meta-learning process, with the goal of generating more diverse training samples to improve the generalization ability of the model. This includes common data augmentation techniques such as random cropping, rotation, and scaling.

MetaMix aimed at enhancing generalization in meta-learning tasks. It employs techniques to improve the model’s capability to handle variations and adapt to new tasks more effectively.

Dropout-Bins utilizes dropout techniques to improve generalization in meta-learning. These techniques enhance model robustness and help mitigate overfitting.

MetaCRL is based on causal inference and explores the task confounder problem existing in meta-learning to eliminate

Table 8. Performance (MSE \pm 95% confidence interval) comparison on pose prediction. The best results are highlighted in **bold**.

MODEL	10-SHOT	15-SHOT
META-TRANS	2.671 \pm 0.248	2.560 \pm 0.196
MR-MAML	2.907 \pm 0.255	2.276 \pm 0.169
MAML	3.113 \pm 0.241	2.496 \pm 0.182
MAML + METAMIX	2.429 \pm 0.198	1.987 \pm 0.151
MAML + DROPOUT-BINS	2.396 \pm 0.209	1.961 \pm 0.134
MAML + METACRL	2.355 \pm 0.200	1.931 \pm 0.134
MAML + TRLEARNER	2.334 \pm 0.216	1.875 \pm 0.132
PROTONET	3.571 \pm 0.215	2.650 \pm 0.210
PROTONET + METAMIX	3.088 \pm 0.204	2.339 \pm 0.197
PROTONET + DROPOUT-BINS	2.761 \pm 0.198	2.011 \pm 0.188
PROTONET + METACRL	2.356 \pm 0.171	1.879 \pm 0.200
PROTONET + TRLEARNER	2.341 \pm 0.150	1.860 \pm 0.354
ANIL	6.921 \pm 0.415	6.602 \pm 0.385
ANIL + METAMIX	6.394 \pm 0.385	6.097 \pm 0.311
ANIL + DROPOUT-BINS	6.289 \pm 0.416	6.064 \pm 0.397
ANIL + METACRL	6.287 \pm 0.401	6.055 \pm 0.339
ANIL + TRLEARNER	6.287 \pm 0.268	6.047 \pm 0.315
METASGD	2.811 \pm 0.239	2.017 \pm 0.182
METASGD + METAMIX	2.388 \pm 0.204	1.952 \pm 0.134
METASGD + DROPOUT-BINS	2.369 \pm 0.217	1.927 \pm 0.120
METASGD + METACRL	2.362 \pm 0.196	1.920 \pm 0.191
METASGD + TRLEARNER	2.357 \pm 0.188	1.893 \pm 0.176
T-NET	2.841 \pm 0.177	2.712 \pm 0.225
T-NET + METAMIX	2.562 \pm 0.280	2.410 \pm 0.192
T-NET + DROPOUT-BINS	2.487 \pm 0.212	2.402 \pm 0.178
T-NET + METACRL	2.481 \pm 0.274	2.400 \pm 0.171
T-NET + TRLEARNER	2.476 \pm 0.248	2.398 \pm 0.167

confusion, improving the generalization and transferability of meta-learning.

Meta-Trans combines transfer learning and meta-learning to fine-tune the pre-trained model to adapt to new tasks. The model is adjusted based on existing knowledge to improve the generalization ability on new tasks.

MR-MAML addresses the bias introduced by task overlap by designing a meta-regularization objective using information theory that prioritizes data-driven adaptation. This leads the meta-learner to decide what must be learned from the task training data and what should be inferred from the task test inputs.

iMOL is proposed for continuously adaptive out-of-distribution (CAOOD) detection, whose goal is to develop an OOD detection model that can dynamically and quickly adapt to emerging distributions and insufficient ID samples during deployment. It is worth noting that in order to adapt iMOL to the tasks of regression, classification, etc. in this paper, we rewrote the loss function of the method.

OOD-MAML is a meta-learning method for out-of-distribution data. It improves the generalization ability of the model by learning tasks on different distributions, especially when facing new distributions.

RotoGBML homogenizes the gradients of OOD tasks, thereby capturing common knowledge from different distributions to improve generalization. RotoGBML uses reweighted vectors to dynamically balance different magnitudes to a common scale, and uses rotation matrices to rotate conflicting directions to be close to each other.

These methods and backbones are critical components of the experimental setup and are used to construct a comprehensive empirical analysis in this paper.

G. Implementation and Architecture

Within the meta-learning framework, we utilize the Conv4 architecture (Finn et al., 2017) as the basis for the feature extractor. After the convolution and filtering steps, we sequentially apply batch normalization, ReLU activation, and 2×2 max pooling

Table 9. Performance (MSE) comparison on the sinusoid regression problem. The “\” denotes that the result is not reported. The best results are highlighted in **bold**.

MODEL	5-SHOT	10-SHOT
MAML	0.593 ± 0.120	0.166 ± 0.061
MAML + METAMIX	0.476 ± 0.109	0.085 ± 0.024
MAML + METACRL	0.440 ± 0.079	0.054 ± 0.018
MAML + METAMIX + METACRL	0.441 ± 0.081	0.053 ± 0.019
MAML + METAMIX + TRLEARNER	0.398 ± 0.047	0.050 ± 0.015
MAML + METACRL + TRLEARNER	0.395 ± 0.050	0.047 ± 0.019
ANIL	0.541 ± 0.118	0.103 ± 0.032
ANIL + METAMIX	0.514 ± 0.106	0.083 ± 0.022
ANIL + METACRL	0.468 ± 0.094	0.081 ± 0.019
ANIL + METAMIX + METACRL	0.465 ± 0.096	0.080 ± 0.019
ANIL + METAMIX + TRLEARNER	0.465 ± 0.090	0.070 ± 0.021
ANIL + METACRL + TRLEARNER	0.462 ± 0.046	0.066 ± 0.021
T-NET	0.564 ± 0.128	0.111 ± 0.042
T-NET + METAMIX	0.498 ± 0.113	0.094 ± 0.025
T-NET + METACRL	0.462 ± 0.078	0.071 ± 0.019
T-NET + METAMIX + METACRL	0.465 ± 0.102	0.077 ± 0.018
T-NET + METAMIX + TRLEARNER	0.440 ± 0.065	0.061 ± 0.012
T-NET + METACRL + TRLEARNER	0.437 ± 0.042	0.054 ± 0.009

Table 10. Performance (accuracy \pm 95% confidence interval) of image classification on Omniglot and miniImagenet. The “\” denotes that the result is not reported. The best results are in **bold**.

MODEL	OMNIGLOT	MINIIMAGENET
MAML	87.15 ± 0.61	33.16 ± 1.70
MAML + METAMIX	91.97 ± 0.51	38.97 ± 1.81
MAML + METACRL	93.00 ± 0.42	41.55 ± 1.76
MAML + METAMIX + METACRL	92.88 ± 0.45	41.57 ± 1.74
MAML + METAMIX + TRLEARNER	94.91 ± 0.61	43.15 ± 1.17
MAML + METACRL + TRLEARNER	95.01 ± 0.71	43.84 ± 1.55
ANIL	89.17 ± 0.56	34.96 ± 1.71
ANIL + METAMIX	92.88 ± 0.51	37.82 ± 1.75
ANIL + METACRL	92.91 ± 0.52	38.55 ± 1.81
ANIL + METAMIX + METACRL	92.99 ± 0.51	38.60 ± 1.79
ANIL + METAMIX + TRLEARNER	93.51 ± 0.48	\
ANIL + METACRL + TRLEARNER	94.13 ± 0.62	\
METASGD	87.81 ± 0.61	33.97 ± 0.92
METASGD + METAMIX	93.44 ± 0.45	40.28 ± 0.96
METASGD + METACRL	94.12 ± 0.43	41.22 ± 0.93
METASGD + METAMIX + METACRL	94.08 ± 0.44	41.20 ± 0.95
METASGD + METAMIX + TRLEARNER	94.62 ± 0.50	\
METASGD + METACRL + TRLEARNER	95.00 ± 0.71	\
T-NET	87.66 ± 0.59	33.69 ± 1.72
T-NET + METAMIX	93.16 ± 0.48	39.18 ± 1.73
T-NET + METACRL	93.81 ± 0.52	40.08 ± 1.74
T-NET + METAMIX + METACRL	93.91 ± 0.52	40.15 ± 1.74
T-NET + METAMIX + TRLEARNER	94.81 ± 0.56	\
T-NET + METACRL + TRLEARNER	95.20 ± 0.47	\

Table 11. Evaluation (accuracy \pm 95% confidence interval) of OOD generalization on Meta-Dataset. The overall results are not the average of ID (in-domain) and OOD (out-of-domain) results, but rather obtained by training on all ten datasets of Meta-Dataset.

MODEL	OVERALL	ID	OOD
MAML	24.51 ± 0.13	31.37 ± 0.09	19.19 ± 0.10
MAML + METAMIX	24.94 ± 0.15	33.91 ± 0.12	20.00 ± 0.11
MAML + METACRL	29.65 ± 0.22	36.56 ± 0.15	24.71 ± 0.14
MAML + TRLEARNER	33.01 ± 0.27	41.12 ± 0.15	29.49 ± 0.12
PROTONET	37.92 ± 0.19	42.18 ± 0.17	30.89 ± 0.11
PROTONET + METAMIX	37.54 ± 0.21	42.56 ± 0.16	31.15 ± 0.13
PROTONET + METACRL	38.91 ± 0.20	44.27 ± 0.14	33.02 ± 0.12
PROTONET + TRLEARNER	40.41 ± 0.21	44.18 ± 0.16	35.15 ± 0.12

(achieved via stride convolutions). The final output from the feature extractor’s last layer is then fed into a softmax layer with N_{tr} heads as classifiers. For one batch of training, we use different heads to participate in the training of task-specific models and introduce relation-aware consistency regularizers to participate in the update of the second layer. These network architectures undergo a pretraining phase and remain unchanged during the training process. Notably, as described in (Jiang et al., 2022), we employ a different architecture for pose prediction experiments. This model consists of a fixed encoder with three convolutional blocks and an adaptive decoder with four convolutional blocks. Each block includes a convolutional layer, batch normalization, and ReLU activation. For the optimization process, we use the Adam optimizer to train our model, with momentum set at 0.8 and weight decay at 0.7×10^{-5} . The initial learning rate for all experiments is 0.1, with the option for linear scaling as needed.

H. Additional Results

In this section, we provide the additional experiments and the full results, including the details of motivating experiments, full results of comparison experiments, results together with task augmentation, trade-off performance comparison, OOD generalization performance comparison, and task relation visualization.

H.1. Details of Motivating Experiment

To validate our hypotheses about the errors of the meta-learning paradigm, we conduct a toy experiment. We randomly select 20 sets of tasks from the miniImagenet dataset (Vinyals et al., 2016) following the method in (Wang et al., 2024a). The adaptive sampler (Wang et al., 2024a) we used here is the same as mentioned in Section 4.1 which aims to sample task-specific meta-data for each task. It conducts three metrics, i.e., task diversity, task entropy and task diffuculty, which considers four important indicators to perform task sampling, i.e., intra-class compaction, inter-class separability, feature space enrichment, and causal invariance. In this experiment, we use the first metric to calculate the score of the 20 sets of sampled tasks. Among these, we select the two tasks with the highest sampling scores as \mathcal{D}_1 - \mathcal{D}_2 and the two with the lowest scores as \mathcal{D}_3 - \mathcal{D}_4 . Higher sampling scores indicate greater task complexity. Next, we perform four-fold data augmentation on \mathcal{D}_1 - \mathcal{D}_2 and evaluate the model’s adaptation on all four sets of tasks by performing a single gradient descent step and recording the training loss and accuracy on previously unseen test tasks. Due to space limitations, we only provide the results of the models trained on \mathcal{D}_1 and \mathcal{D}_4 in Figure 2. Here, we provide all four groups of results in Figure 6. From the results, we can see that the model obtains similar results on \mathcal{D}_1 and \mathcal{D}_2 as the main text: models show reduced effectiveness post-convergence but exhibit gradually improving test performance, suggesting underfitting. Meanwhile, for the performance of models on \mathcal{D}_3 and \mathcal{D}_4 , we can observe that as the number of training epochs increases, the performance on base classes gradually improves; however, the performance on the new classes first increases and then decreases. The phenomenon is consistent with the definition of overfitting. Therefore, the meta-learning models may face underfitting or overfitting problems depending on the tasks.

Considering the randomness in the model training process, we further sample eight sets of data and evaluate the model’s training performance before and after introducing TRLearner. Specifically, we use all three metrics in (Wang et al., 2024a) to calculate the score of the 40 sets of sampled tasks. We identify the top four tasks with the highest scores as \mathcal{D}_1 to \mathcal{D}_4 , and the bottom four tasks as \mathcal{D}_5 to \mathcal{D}_8 . Higher sampling scores indicate more complex tasks, providing the model with more information. We then apply four-fold data augmentation to \mathcal{D}_1 to \mathcal{D}_4 . Finally, we assess the MAML model’s adaptation on these eight task sets by performing a single gradient descent and recording the accuracy. Ideally, \mathcal{D}_1 to \mathcal{D}_4 not only contain more information, but also further enhance the sample diversity through augmentation. Therefore, the model performs better after training on these four groups of tasks, and there is no overfitting. However, as shown in Figure 7 middle, in the initial stage of the model, that is, under the constraint of limited training time, the model will be lower than the effect of training on \mathcal{D}_5 to \mathcal{D}_8 . Therefore, it will face the limitation of underfitting since it only performs one step of gradient optimization. This further verifies our point of view, i.e., MAML has the limitations of overfitting and underfitting which is caused by its own learning paradigm. Further, in order to evaluate the impact of introducing TRLearner on the model, we experimented with MAML+TRLearner under the same setting. The results are shown in Figure 7. The results show that after the introduction of TRLearner, the overfitting and underfitting phenomena of the model are greatly alleviated.

H.2. Full Results of Comparison Experiments

We provide a comprehensive set of experimental results for the scenarios of image classification, drug activity prediction, and pose prediction in Table 6, Table 7, and Table 8, respectively. The specific experimental configurations for these three

scenarios are detailed in Section 6, with further elaboration available in the appendix. The findings confirm that, as expected, introducing TRLearner consistently delivers comparable performance across all cases.

H.3. Results Together with Other Regularizers

Although the regularization methods we choose all focus on the generalization of meta-learning, they each consider different aspects such as task augmentation and task confounder. Depending on the differences between different scenarios, the use of different solutions varies greatly. e.g., the research insights proposed in (Yao et al., 2021) show that data augmentation improves the model more significantly in the pose prediction scenario. Therefore, in order to further evaluate the potential of our method, we introduce TRLearner on the basis of introducing the regularization baselines. The results are shown in Tables 9 and 10. We can observe that the introduction of TRLearner achieves continuous and stable improvements. Therefore, our work focuses on the task relation that has been ignored by previous methods, while effectively improving the generalization.

H.4. Trade-off Performance Comparison

According to the above analysis, TRLearner improves the generalization of meta-learning in multiple scenarios. Considering that TRLearner may bring additional computational overhead due to the introduction of regularization terms, we evaluate the trade-off performance after introducing TRLearner to ensure the actual effect of TRLearner. Specifically, we use MAML as a baseline, conduct experiments on the miniImagenet dataset, and evaluate its accuracy, training time, and parameter size after introducing different methods. Figure 8 shows the trade-off performance. From the results, we can observe that after introducing TRLearner, the model achieves a significant performance improvement with acceptable calculational cost and parameter size compared to the original framework. Compared with the other baselines, it even achieves faster convergence on the basis of the effect advantage.

H.5. OOD Generalization Performance Comparison

To demonstrate the effect of TRLearner on improving generalization ability, we strengthened the distribution difference between training and testing tasks to evaluate its improvement on OOD generalization of meta-learning.

Specifically, in addition to the classification experiments in the cross-domain few-shot learning scenario, we also select a set of benchmark datasets that are most commonly used for OOD generalization verification, i.e., Meta-dataset (Triantafillou et al., 2019). This benchmark serves as a substantial resource for few-shot learning, encompassing a total of 10 datasets that span a variety of distinct domains. It is crafted to reflect a more authentic scenario by not confining few-shot tasks to a rigid set of ways and shots. The dataset encompasses 10 varied domains, with the initial 8 in-domain (ID) datasets designated for meta-training, which include ILSVRC, Omniglot, Aircraft, Birds, Textures, Quick Draw, Fungi, and VGG Flower. The final 2 datasets are earmarked for assessing out-of-domain (OOD) performance, namely Traffic Signs and MSCOCO. We assess the efficacy of meta-learning models across these 10 domains, utilizing diverse samplers across the entire suite of 10 datasets. We first sample the metadata of training and testing tasks based on the adaptive sampler (Wang et al., 2024a). Then, we record the performance changes of the meta-learning model before and after the introduction of TRLearner.

From the results in Table 11, we can observe that after the introduction of TRLearner, meta-learning achieves a significant performance improvement, reaching 4% on average. This further illustrates the effect of task relation on OOD generalization.

H.6. Task Relation Visualization

In this subsection, we visualize the task relation extracted by TRLearner. Specifically, we visualize the initialized task relation matrix, the task relation matrix directly calculated based on the extracted task-specific meta-data, and the task relation matrix further learned using a multi-headed similarity layer. Taking miniImagenet as an example, we set a training batch including 4 tasks and visualize the matrix and model effect after 100 epochs of training. The visualization results are shown in Figure 9. We can observe that the task relation matrix learned based on the multi-headed similarity layer is more accurate, and the meta-learning model learned based on it has the best effect. The results demonstrate the effect of TRLearner and the importance of task relations.

H.7. Performance Under Different Meta-Layer

TRLearner enhances important feature learning by leveraging task relationships, improving the performance of meta-learning models. As described in Subsection 3.2, its design aims to identify a proxy that enables accurate decisions even under

modeling errors. Previous experiments have demonstrated TRLearner’s performance improvements. To further verify its ability to mitigate modeling errors, we design a set of experiments in this subsection to evaluate the performance of meta-learning models using TRLearner under different meta-layer configurations.

Specifically, we adopt the same experimental setup as in Subsection 6.2, evaluating on the miniImagenet dataset. MAML is selected as the baseline algorithm, with the meta-layer depth set to 1, 4, 8, and 16, respectively, and trained on miniImagenet. Notably, these four configurations share identical training and testing data, differing only in model architecture. According to (Mohri, 2018), the optimal structure for a specific task varies depending on the task. Models with optimal structures can fully learn task features to support accurate predictions. However, as shown in the experimental results in Figure 10, the introduction of TRLearner eliminates significant differences in MAML’s performance across the four meta-layer settings. This indicates that TRLearner mitigates modeling errors arising from meta-layer depth selection, further demonstrating its effectiveness.

I. More Discussion about Uniqueness of TRLearner

TRLearner is the first approach to leverage inter-task relationships to guide the optimization process in meta-learning from the perspective of learning lens, a consideration overlooked by previous work. While other fields have also explored introducing task-level information to improve model performance—such as cross-task validation and many-shot knowledge distillation—there are essential conceptual differences between these methods and TRLearner. Previous methods often focus on intra-task category relationships or use task performance as a validation tool. In contrast, TRLearner directly incorporates inter-task relationships into the optimization process, thus avoiding the pitfall of indiscriminately absorbing all information.

More specifically, cross-task validation (Anderson, 1972; Kung et al., 2023; Wang et al., 2024b; Appel et al., 2021; Kim et al., 2023) typically involves using the performance of auxiliary tasks during the meta-learning training phase to validate and regulate the main task’s learning. Essentially, it serves as an evaluation and monitoring mechanism during training rather than transmitting inter-task knowledge to enhance the model’s adaptability to new tasks. Many-shot knowledge distillation (Sauer et al., 2022; Li et al., 2021; Zhao et al., 2023; Iscen et al., 2021) mainly emphasizes aggregating knowledge from multiple sources (e.g., multiple teacher models or tasks with varying scales and perspectives) to provide rich informational inputs to a student model. However, it does not specifically emphasize selective filtering of task information or the utilization of inter-task structural relationships. As a result, the model may indiscriminately absorb all incoming information, increasing optimization difficulty and potentially introducing irrelevant features. In contrast, TRLearner’s key innovation lies in its deep exploration and exploitation of inter-task correlations and commonalities, enabling the method to selectively and conditionally incorporate multi-task information. By leveraging an explicit inter-task relational structure, TRLearner can extract useful information from other tasks when data is scarce, thereby improving learning efficiency. Conversely, when data is abundant, it can filter out irrelevant factors and focus attention on the shared information most beneficial for the new task. Under varying data conditions, TRLearner consistently achieves stronger generalization and robustness. This feature not only emphasizes effective utilization of multi-task information but also ensures that optimization is guided by inter-task relationships, thus establishing a uniquely efficient paradigm for knowledge transfer and adaptation in meta-learning.